PUBLISHER :

Address of Publisher
& Editor's Office :

GDAŃSK UNIVERSITY
OF TECHNOLOGY
Faculty
of Ocean Engineering
& Ship Technology

ul. Narutowicza 11/12
80-952 Gdańsk, POLAND
tel.: +48 58 347 13 66
fax : +48 58 341 47 12
e-mail : office.pmr@pg.gda.pl

Account number :
BANK ZACHODNI WBK S.A.
I Oddział w Gdańsku
41 1090 1098 0000 0000 0901 5569

Editorial Staff :
Witold Kirkor Editor in Chief
e-mail : pmrs@op.pl
Przemysław Wierzchowski Scientific Editor
e-mail : e.wierzchowski@chello.pl
Piotr Bzura Editor for review matters
e-mail : pbzura@pg.gda.pl
Tadeusz Borzęcki Editor for international relations
e-mail : tadbor@pg.gda.pl
Kazimierz Kempa Managing Editor
e-mail : kkempa@pg.gda.pl
Cezary Spigarski Computer Design
e-mail : biuro@oficynamorska.pl

Domestic price :
single issue : 20 zł

Prices for abroad :
single issue :
- in Europe EURO 15
- overseas US$ 20

ISSN 1233-2585

POLISH MARITIME RESEARCH
in internet
www.bg.pg.gda.pl/pmr.html

POLISH MARITIME RESEARCH
No 2(52) 2007 Vol 14

CONTENTS

The papers published in this issue have been reviewed by :
Assoc.Prof. Z. Chłopek ; Assoc. Prof. M. Sperski
Prof. J. Szantyr ; Prof. S. Szczeciński

Editorial

POLISH MARITIME RESEARCH is a scientific journal of worldwide circulation. The journal appears as a quarterly four times a year. The first issue of it was published in September 1994. Its main aim is to present original, innovative scientific ideas and Research & Development achievements in the field of :

Engineering, **Computing & Technology**, **Mechanical Engineering**,

which could find applications in the broad domain of maritime economy. Hence there are published papers which concern methods of the designing, manufacturing and operating processes of such technical objects and devices as : ships, port equipment, ocean engineering units, underwater vehicles and equipment as well as harbour facilities, with accounting for marine environment protection.
The Editors of POLISH MARITIME RESEARCH make also efforts to present problems dealing with education of engineers and scientific and teaching personnel. As a rule, the basic papers are supplemented by information on conferences , important scientific events as well as cooperation in carrying out international scientific research projects.

Scientific Board

Manoeuvring forces on azimuthing podded propulsor model

Maciej Reichel
Ship Design and Research Centre
(CTO S.A.) Gdańsk

ABSTRACT

This paper presents the preliminary part of comprehensive manoeuvring open- water tests of a gas carrier model. The paper focuses on open water experiments with an azimuthing podded propulsor. The test program was carried out in the cavitation tunnel and the large towing tank of Ship Hydromechanics Division, Ship Design and Research Centre, Gdańsk. The pod was tested as a pushing unit with a 161.3 mm diameter propeller. Steering forces were measured in the range of advance coefficient from 0.0 to 0.8 combined with the range of deflection angles from -45° up to +45°. Measurements on the pod without propeller were also performed. The experiment results are presented in the form of non-dimensional coefficients in function of advance coefficient and deflection angle. Analysis of the experimental results and the conclusions are presented.

Keywords : podded propulsors, open water experiments, manoeuvring forces.

INTRODUCTION

Podded propulsion, an integrated propulsion and steering system is known for nearly half a century [1].This type of propulsion has many advantages in comparison with traditional propeller-rudder set, e.g. vibration reduction and flexibility of internal design arrangement. But the most important advantage is its better manoeuvrability.

Although the good manoeuvring abilities of podded ships are known the manoeuvring characteristics are still not fully recognized. Standard experiments with free running propellers are not sufficient because the interaction effects between propeller and pod housing are very difficult to predict. Therefore it is advisable to carry out model tests with different podded drives to get data basis for the forces and moments at different steering angles [2, 3]. It is important to collect data for many possible pod configurations, e.g. push, pull, single or twin set.

The knowledge of the forces and moments acting on the propeller and podded drive at different steering angles is necessary for design and optimisation of azimuthing propulsion systems. Also information about wake velocity field is important in design aft part of the hull and possibly also skegs or additional rudders [4].

MODEL OF THE PODDED DRIVE

Tab. 1. *Main data of P447 propeller model .*

	Symbol	Unit	Model
Propeller diameter	D	mm	161.3
Pitch at r/R = 0.7	P	mm	126.0
Pitch ratio at r/R = 0.7	P/D	-	0.785
Expanded blade area ratio	A_E/A_0	-	0.550
Hub ratio	d_h/D	-	0.219
Number of blades	z	-	4
Direction of rotation		-	right
Revolutions per minute	n	-	900

Tab. 2. *Main data of POD 09 pod model .*

	Symbol	Unit	Model
Gondola length	l_G	mm	106.2
Gondola diameter	d_G	mm	61.6
Strut height (from propeller shaft)	h	mm	97.6
Strut length	$c_{0.7}$	mm	53.5

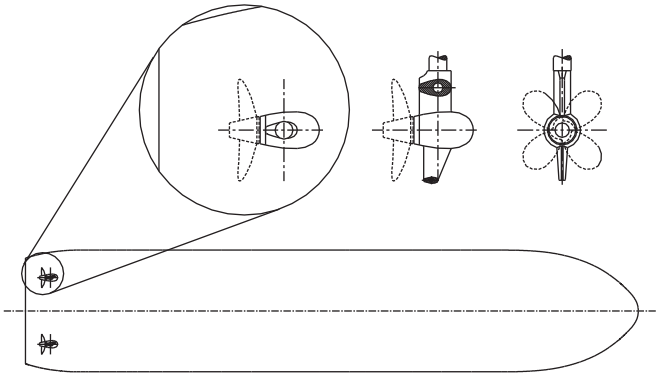

Fig. 1. *Arrangement of pod propulsors and pod geometry .*

TEST FACILITY AND PLAN OF THE EXPERIMENT

The open water tests were carried out in the cavitation tunnel and in the large towing tank of Ship Hydromechanics Division, Ship Design and Research Centre in Gdańsk, (OHO-CTO).

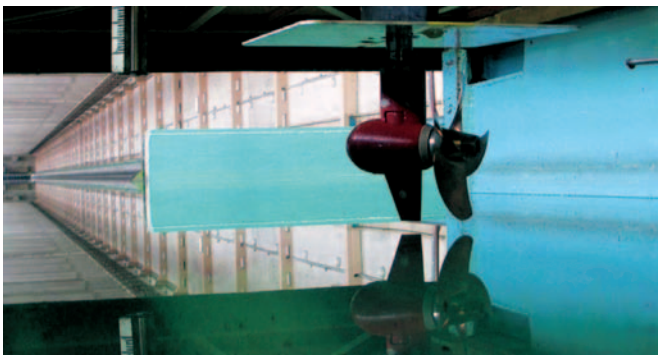

Fig. 2. Podded drive in the OHO-CTO large towing tank before tests .

Measurements were conducted at the constant number of revolutions equal to 900 rpm. The carriage velocities were so established as to obtain advance coefficient of 0.2; 0.4; 0.6; 0.8. The experiments were performed for thirteen deflection angles in the range from -45°up to +45°, with the step of 5° from -15°to +15°and 10 within the rest of the range. Forces on the bare pod, i.e. without propeller, were also measured. The positive deflection angle and directions of forces are shown in Fig.3.

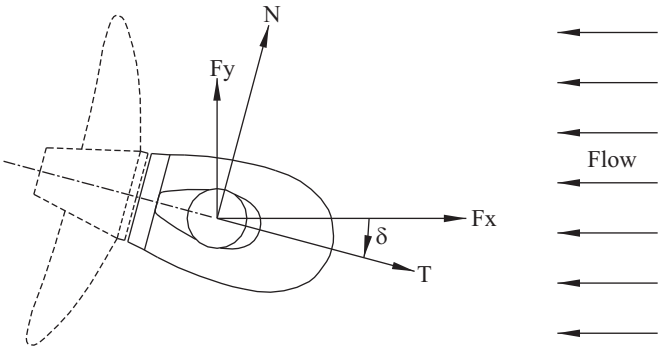

Fig. 3. Definition of forces .

RESULTS

All the results are presented in the traditional non-dimensional form by applying the following formulae :

➡ Advance coefficient $$J = \frac{U_{ref}}{nD} \quad (1)$$

➡ Longitudinal force coefficient $$K_{FX} = \frac{F_X}{\rho n^2 D^4} \quad (2)$$

➡ Transverse force coefficient $$K_{FY} = \frac{F_Y}{\rho n^2 D^4} \quad (3)$$

➡ Thrust coefficient $$K_T = \frac{T}{\rho n^2 D^4} \quad (4)$$

➡ Normal force coefficient $$K_N = \frac{N}{\rho n^2 D^4} \quad (5)$$

➡ Torque coefficient $$K_Q = \frac{Q}{\rho n^2 D^4} \quad (6)$$

where :

U_{ref} - inflow velocity
δ - deflection angle
ρ - water density
n - propeller revolutions
D - propeller diameter.

The thrust and normal force were calculated by applying the following transformation from the towing tank coordinate system to the propulsor coordinate system :

$$\begin{bmatrix} T \\ N \end{bmatrix} = \begin{bmatrix} \cos\delta & -\sin\delta \\ \sin\delta & \cos\delta \end{bmatrix} \begin{bmatrix} F_X \\ F_Y \end{bmatrix}$$

In Fig.4 the open water characteristics for the P447 propeller are shown. The characteristics were measured on the model without pod housing and only for straight flow.

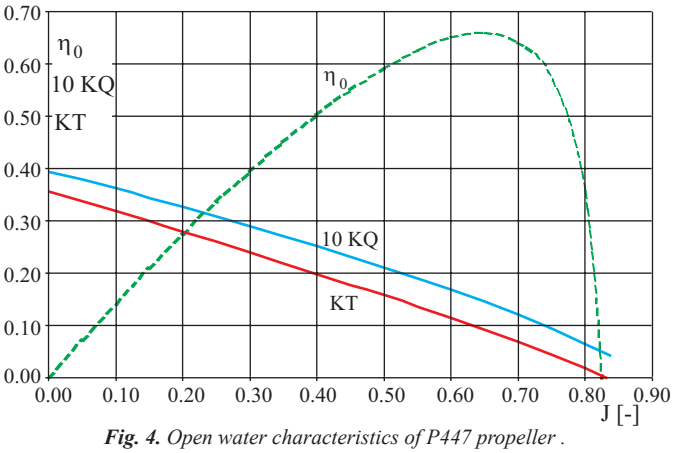

Fig. 4. Open water characteristics of P447 propeller .

Results of the measurements of the forces on the bare pod are presented in the figures below. The experiment was made for one advance coefficient equal to 0.6 and for five deflection angle values : ±45°, ±10°, 0°.

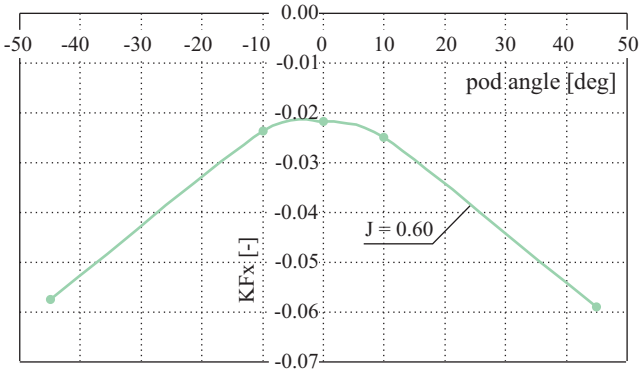

Fig. 5. Longitudinal force coefficients vs. deflection angle of bare pod .

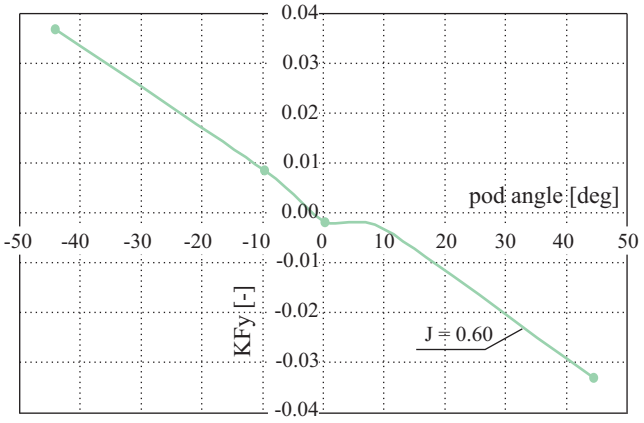

Fig. 6. Transverse force coefficients vs. deflection angle of bare pod .

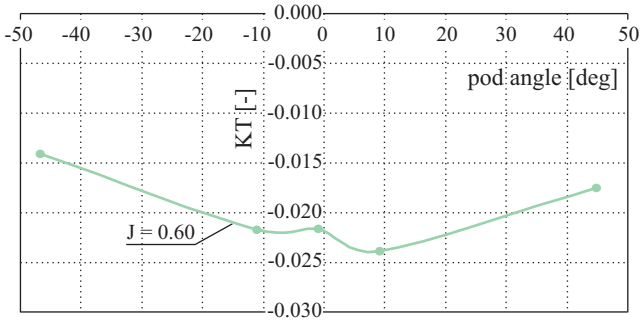

Fig. 7. Thrust force coefficients vs. deflection angle of bare pod .

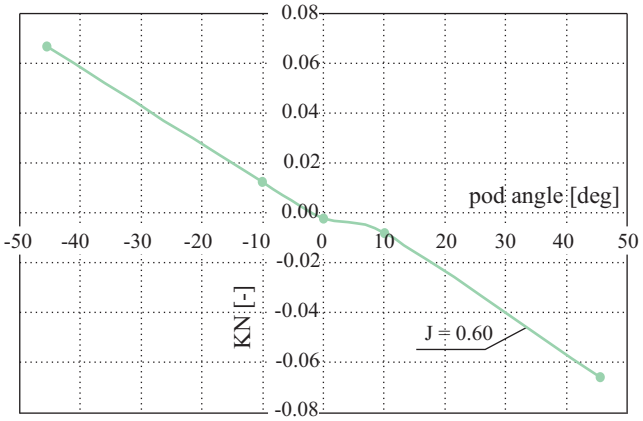

Fig. 8. Normal force coefficients vs. deflection angle of bare pod .

The subsequent figures show results for the podded drive with right-handed P447 propeller.

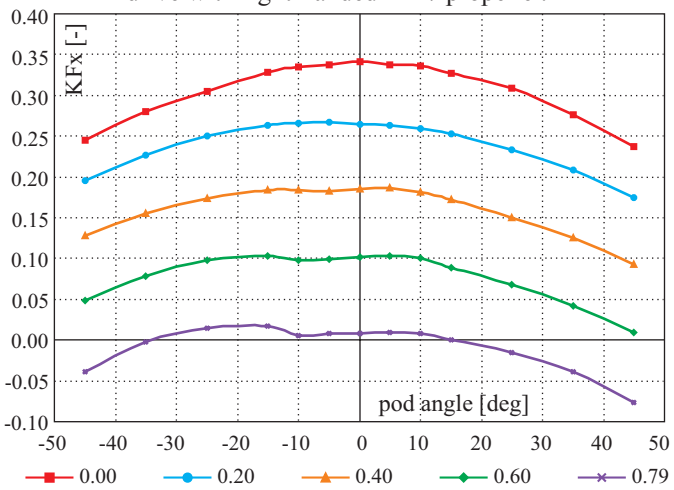

Fig. 9. Longitudinal force coefficient vs. deflection angle .

★ the longitudinal force coefficients show parabolic dependence on deflection angle, with the tendency to reduction for higher angles. For positive deflection angles the reduction of longitudinal force coefficients is higher than for negative ones (Fig.9)

★ the transverse force coefficients are approximately linear in function of deflection angles, with deviation to higher values for larger deflection angles and advance coefficients. In the vicinity of 15° deflection angle a little disturbance is observed (Fig.10)

★ the thrust coefficients depend strongly on deflection angles and propeller loading. For both steering directions the thrust is increasing but its increase is visibly stronger for negative deflection angles (Fig.11)

★ the normal force coefficients behave like the transverse force coefficients, i.e. approximately linear in function of

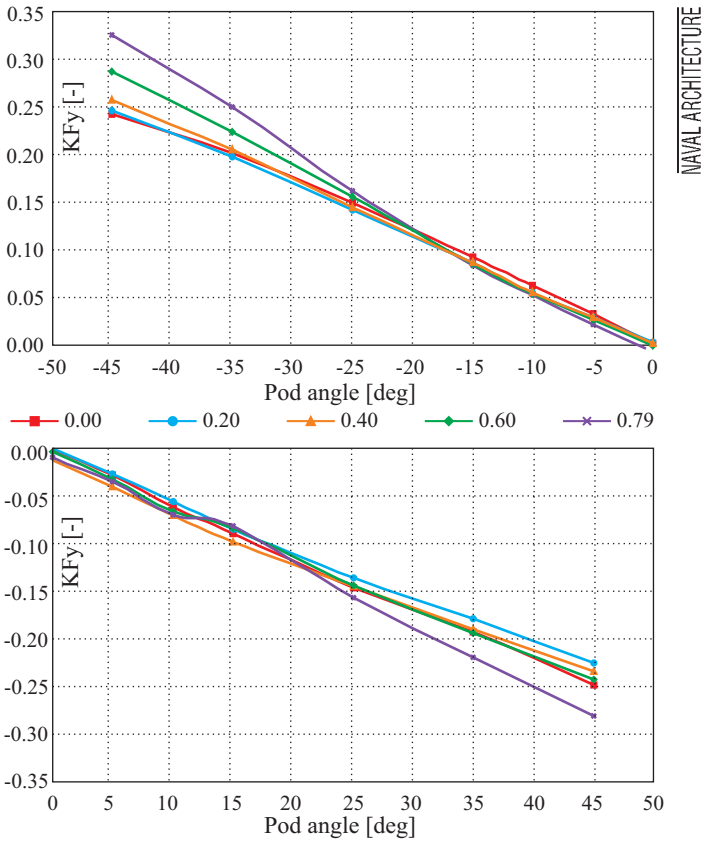

Fig. 10. Transverse force coefficient vs. deflection angle .

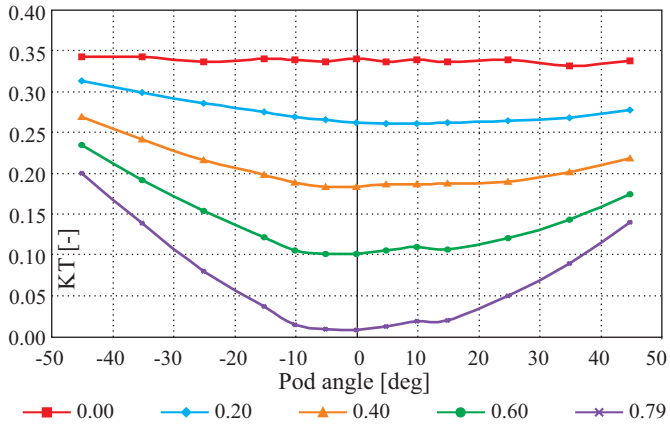

Fig. 11. Thrust coefficient vs. deflection angle .

deflection angle, however with a faster increase for higher advance coefficients. Like in the case of the transverse force coefficients a little disturbance is visible in the vicinity of 15° deflection angle (Fig.12).

To calculate the coefficients of forces in function of advance coefficient the following formulae were applied :

$$U_{ref} = U_{CAR} \cdot \cos\delta \qquad (7)$$

where :

U_{CAR} - towing carriage velocity.

★ for smaller pod deflection angles the longitudinal force coefficients are decreasing faster than for higher ones. The nature of the dependence is similar to that of a classic propeller (Fig.13)

★ for small pod deflection angles up to 15°, the transverse force coefficients depend almost linearly on advance co-

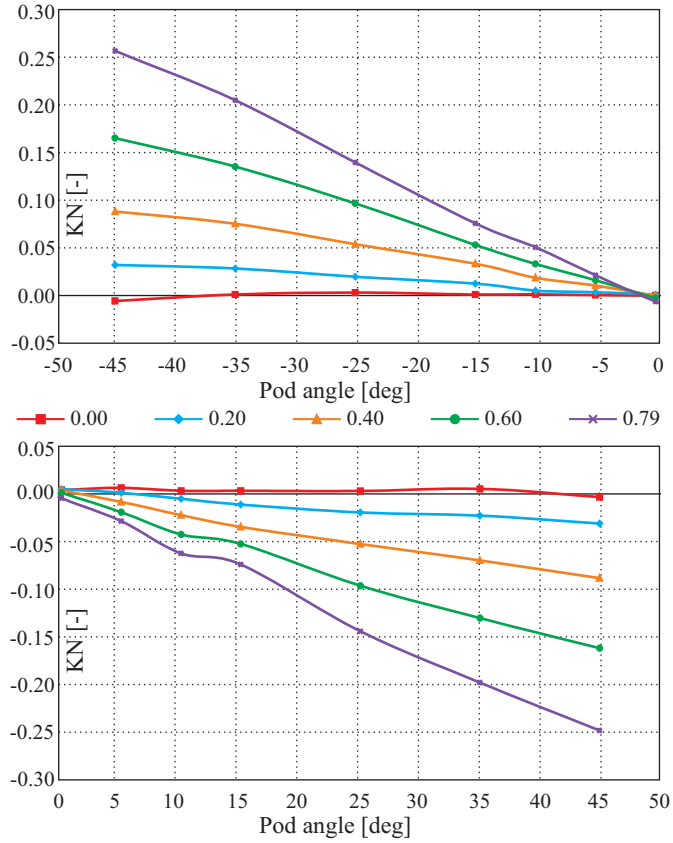

Fig. 12. Normal force coefficient vs. deflection angle .

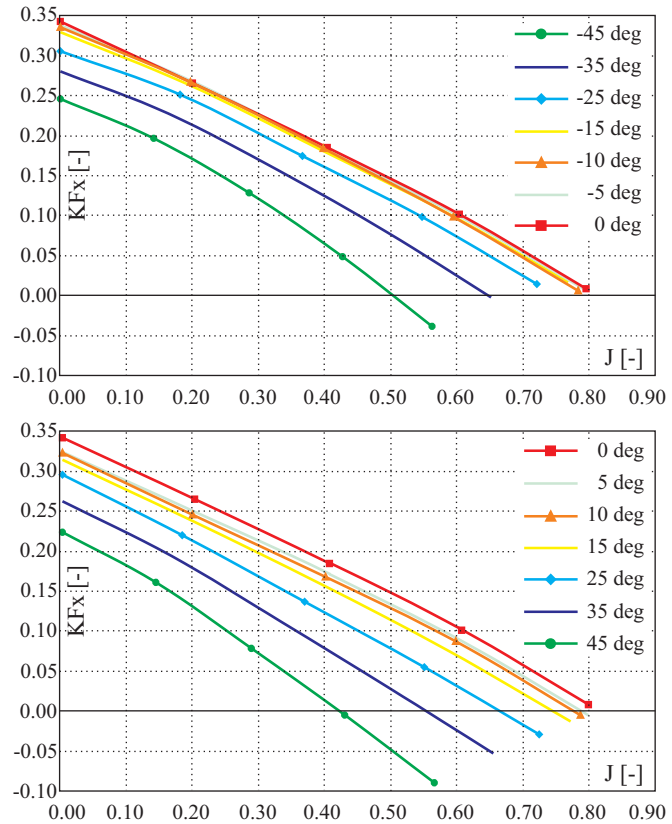

Fig. 13. Longitudinal force coefficient vs. advance coefficient .

efficient; for higher angles the dependence is changing to parabolic one (Fig.14)

★ the thrust coefficients in function of advance coefficient are decreasing but for positive pod deflection angles the decreasing is independent on deflection angle value (Fig.15)

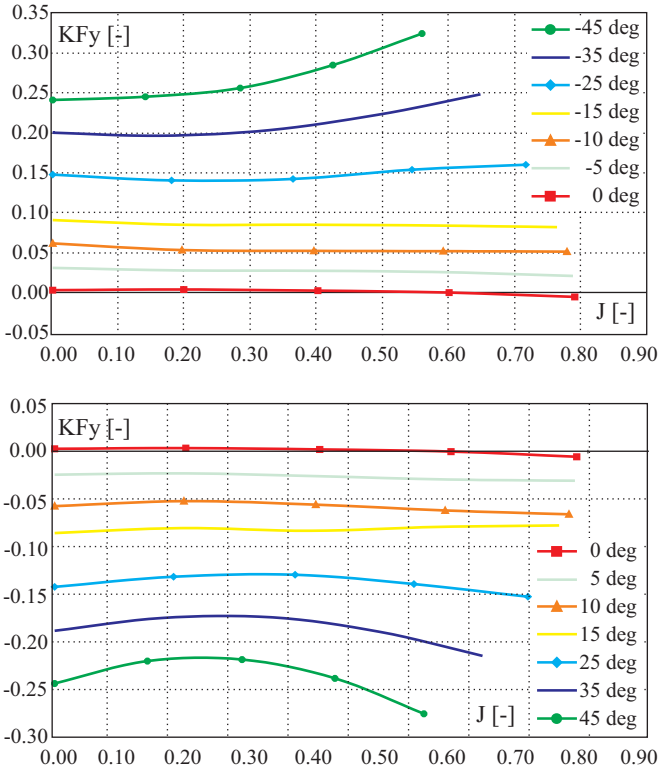

Fig. 14. Transverse force coefficient vs. advance coefficient .

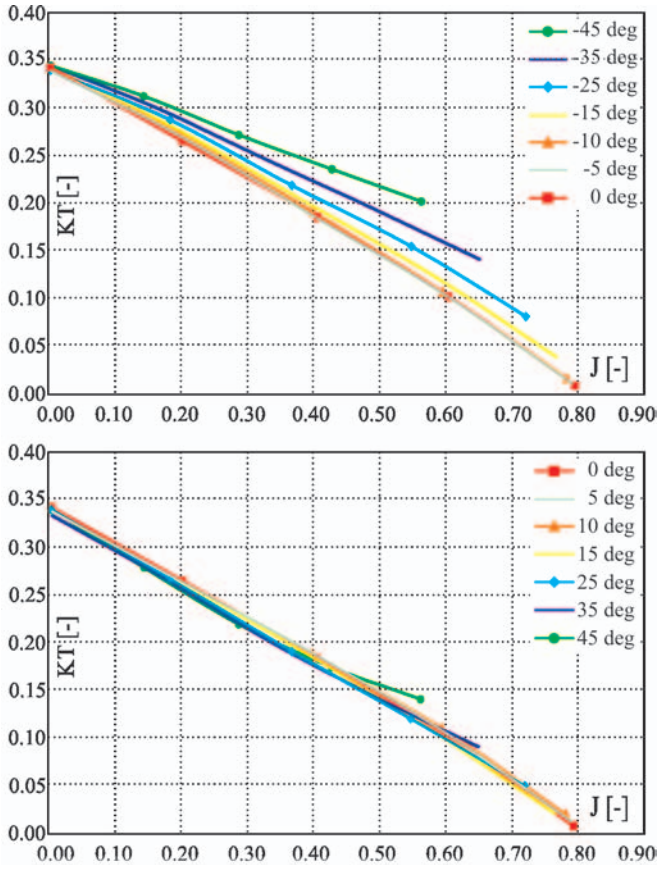

Fig. 15. Thrust coefficient vs. advance coefficient .

★ the normal force coefficients show tendency to change their character from linear to parabolic for higher pod deflection angles in function of advance coefficient (Fig.16)

Fig.17 introduced to summarize the content of the previous figures shows proportion of thrust force and normal force

between positive and negative pod angle. The value of 100% represents the thrust force and normal force for the positive direction of pod angle. For the negative pod deflection angles the absolute value of normal force was used.

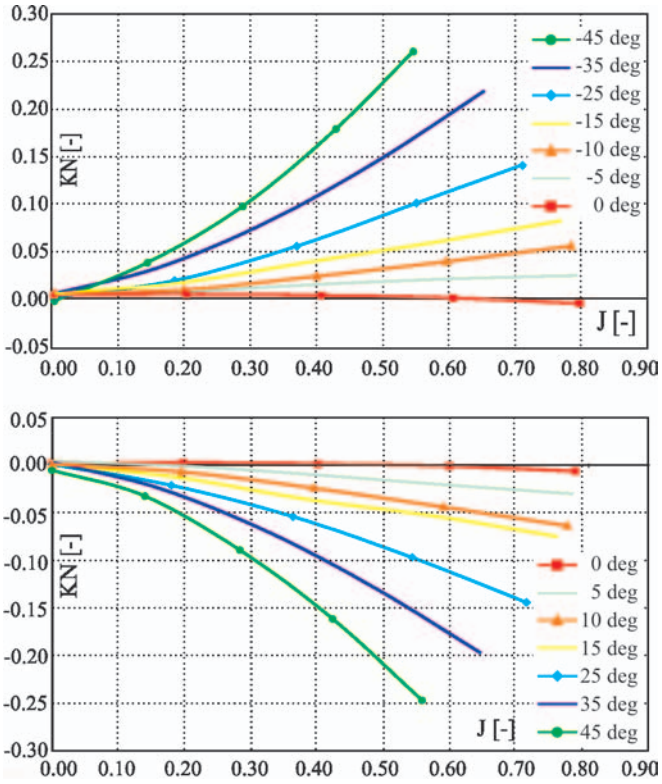

Fig. 16. Normal force coefficient vs. advance coefficient .

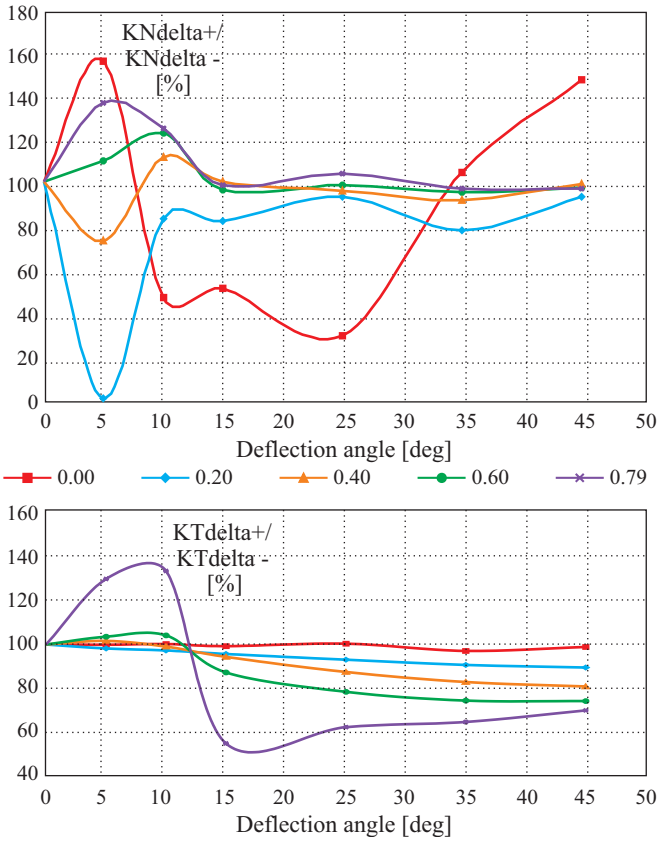

Fig. 17. Interdependence between KT and KN for positive and negative deflection angles

★ the ratio of normal force coefficients shows difficult dependence for small deflection angles, for angles higher than 15° the relationship shows tendency to be linear in the vicinity of in the range of 80 – 100 % $\frac{K N_{\delta+}}{K N_{\delta-}}$. The exception to the tendencies is visible at J = 0.00. For small advance coefficients the normal force coefficient ratio is smaller than for higher ones

★ the ratio of the thrust coefficients shows tendency to increase for small pod angles up to 10°, and to decrease for higher deflection angles. This tendency is more visible for higher advance coefficients.

CONCLUSIONS

To summarize results obtained from the towing tank tests the following conclusions may be presented :

- the presented results clearly show the typical hydrodynamic characteristics of azimuthing podded propulsion
- the asymmetries in values of the force coefficients for positive and negative deflection angles are due to the influence of the direction of propeller rotation (to the right)
- with positive pod angle a negative normal force is produced and vice versa, which results in a destabilizing moment tending to increase the turn rate
- the increase of thrust coefficients for higher deflection angles is induced by reduction of axial inflow velocity which involves reduction of advance coefficient
- for deflection angles larger than 15° the thrust and normal force coefficients are from 10% to 30% smaller than for the corresponding positive deflection angles, which is caused due to the interaction between right – handed propeller and podded drive.

Acknowledgments

The author would like to express his gratitude to the Ship Hydromechanics Division, Ship Design and Research Centre, Gdańsk, especially to Mr. Wojciech Górski, the head of the Division.

NOMENCLATURE

A_E/A_0 - expanded blade area ratio
$c_{0.7}$ - strut length
d_G - gondola diameter
d_h/D - hub ratio
D - propeller diameter
Fx - longitudinal force
Fy - transverse force
h - strut height (from propeller shaft)
J - advance coefficient
K_{FX} - longitudinal force coefficient
K_{FY} - transverse force coefficient
K_N - normal force coefficient
K_Q - torque coefficient
K_T - thrust coefficient
l_G - gondola length
n - revolutions per minute
N - normal force
P - pitch at r/R=0.7
P/D - pitch ratio at r/R=0.7
Q - torque
T - thrust force
U_{CAR} - carriage velocity
U_{ref} - inflow velocity
z - number of blades

δ - pod angle
ρ - water density

BIBLIOGRAPHY

1. Van Terwisga T., Quadvlieg F., Valkhof H.: *Steerable propulsion units: hydrodynamic issues and design consequences.* 80th anniversary of Schottel GmbH & Co., 2001
2. Grygorowicz M., Szantyr J.A. : *Open water experiments with two pod propulsor models.* First International Conference on Technological Advances in Azimuthing Podded Propulsion (T-POD), Newcastle-upon-Tyne, 2004
3. Heinke H. J.: *Investigations about forces and moments at podded drives.* First International Conference on Technological Advances in Azimuthing Podded Propulsion (T-POD), Newcastle-upon-Tyne, 2004
4. Stettler J. W., Hover F.S., Triantafyllou M.S.: *Preliminary results of testing on the dynamics of an azimuthing podded propulsor relating to vehicle maneuvering.* Naval Engineering And Research Consortium, Massachusetts Institute of Technology, 2004.

CONTACT WITH THE AUTHOR

Maciej Reichel, D.Sc., Eng.
Ship Hydromechanics Division,
Ship Design and Research Centre – Stock Company
(OHO - CTO)
Szczecińska 65
80-392 Gdańsk, POLAND
e-mail : maciej.reichel@cto.gda.pl

Conference

REGIONAL GROUP of the Section on Exploitation Foundations

On 18 January 2007 at Mechanical Faculty, Gdynia Maritime University, was held a scientific seminar of the Regional Group of the Section on Exploitation Foundations, Machine Building Committee, Polish Academy of Sciences (PAS).

The Seminar program contained presentation of six papers elaborated by scientific workers of the Faculty, as follows :

- *Professor Jan Kazimierz Włodarski – 55 years of activity in the field : construction and operation of machines* – by R. Cwilewicz and K. Witkowski
- *On failures of piston-cylinder system of ship internal combustion engines* – by J. K. Włodarski
- *Assessment of influence of indicator channel and its dimensions on results of pressure measurements in engine cylinder* – by W. Gałecki
- *Investigations of ageing process of lubricating oils in trunk-piston engines* – by A. Młynarczak
- *Possibilities of diagnosing selected failures of injection devices of self-ignition engines on the basis of indicator diagram run* – by R. Pawletko
- *A new concept of building ship power plant simulators with the use of 3D visualization* – by L. Tomczak

After interesting discussion the Seminar participants visited scientific laboratories of the University.

Miscellanea

Jubilee of 50th Anniversary

On 30 June – 1 July 2006 the Experimental Centre for Ship Model Tests in Open Waters, Faculty of Ocean Engineering and Ship Technology, Gdańsk University of Technology, celebrated 50th anniversary of its rich activity.

The Centre has been established due to initiative of Prof. Lech Kobyliński, Head of the then Ship Theory Department, Faculty of Ocean Engineering and Ship Technology, Gdańsk University of Technology. All the matter have started from hydrofoils. In 1955 a small, 4.5 m long, hydrofoil was built in the Department, whose first trials was conducted on Motława river, and simultaneously the Department was assigned to conduct realization of a project for development of hydrofoils, in which Polish Navy was interested. In that time Prof. Kobyliński decided to organize the Experimental Centre on the area of a deserted water sport centre by Jeziorak lake in Iława. In summer 1956 just in this place the research trials on hydrofoils started again. Results of the research on a few manned models as well as relevant theoretical elaborations resulted in the mastering of design principles of such floating units.

In 1965 in Wisła Shipyard was built a passenger hydrofoil for 76 persons, which was operated by Szczecin Coastal Shipping Co till 1968, and after modernization - by Polish Navy on the Gdynia - Hel route till 1993. Finally the activity in that area was ended in the 1960s when several hydrofoils were purchased in Soviet Union. Apart from hydrofoils, model tests started in the range of resistance, propulsion, propellers, manoeuvrability, sea-keeping qualities of conventional ships, and also of river pushers and push-trains, hovercrafts and fast boats; also various special investigations were carried out there.

Results of the tests were implemented by shipyards' ship design offices, shipping companies and classification institutions, as well as they were presented at many scientific conferences in Poland and abroad.

25 years ago, also in Iława, has started the first ship manoeuvring training course for ship masters, carried out with the use of large manned ship models, that contributed to arranging the Training Centre by the Silm lake.

These services and research carried out in Iława have initiated organization of symposia on ship hydromechanics in Poland, and later - also symposia on ship manoeuvrability.

Hence it is not an exaggeration to state that the Centre in question deserves the name of the "cradle" of Polish ship hydromechanics.

In present, the Centre fulfils also the role of the base for international student scientific camps, and permanently, the student training base for yachting sports.

On the fatigue-critical amplitude of random-amplitude stress

Janusz Kolenda
Gdańsk University of Technology
Polish Naval University

ABSTRACT

Uniaxial non-zero mean stress of constant circular frequency in the high-cycle fatigue regime is considered. It is assumed that equation of the S-N curve and modified Soderberg equation are applicable. For constant-amplitude stress, the fatigue-critical stress amplitude is defined as that which leads to failure during the required design life. For random-amplitude stress, expected values of the fatigue-critical stress amplitude and total fatigue damage accumulated during the required design life are estimated. It is found that the probability of fatigue failure is equal to the probability of exceedance of the fatigue-critical stress amplitude. As an example, for stationary random stress the equivalent random-amplitude stress and probability of fatigue failure are determined.

Key words : uniaxial load, random stress, high-cycle fatigue, failure probability

INTRODUCTION

If a metallic element is subjected to asymmetric tensile-compressive stress

$$\tilde{\sigma}(t) = \sigma_0 + \sigma_a \sin \omega t \tag{1}$$

in the high-cycle fatigue regime the following equations are frequently applied [1, 2]

$$N\sigma^m = K \tag{2}$$

$$\sigma_a = \sigma\left(1 - \frac{\sigma_0}{R_e}\right) \quad , \quad Z_{rc} < \sigma \le L \tag{3}$$

where :

- K – fatigue strength coefficient
- L – maximum stress amplitude satisfying Eq. (2) (above which low-cycle fatigue may occur)
- m – fatigue strength exponent
- N – number of cycles to cause fatigue failure
- R_e – tensile yield strength
- Z_{rc} – fatigue limit under fully reversed tension-compression
- σ – amplitude of the fully reversed stress at a given number, N, of cycles to cause failure
- σ_a – amplitude of the stress (1) which will give that fatigue life
- σ_0 – mean stress
- ω – circular frequency.

If N_d denotes the required cycle number the design criterion $N_d < N$ becomes :

$$\frac{N_d}{K}\left(\frac{\sigma_a}{1 - \frac{\sigma_0}{R_e}}\right)^m < 1 \tag{4}$$

for :

$$Z_{rc}\left(1 - \frac{\sigma_0}{R_e}\right) < \sigma_a \le L\left(1 - \frac{\sigma_0}{R_e}\right)$$

Hence the stress amplitude σ_{cr} that leads to fatigue failure in N_d cycles is :

$$\sigma_{cr} = \left(1 - \frac{\sigma_0}{R_e}\right)\left(\frac{K}{N_d}\right)^{1/m} \tag{5}$$

This quantity will be called the fatigue-critical stress amplitude.

DESIGN CRITERION AT STATIONARY RANDOM-AMPLITUDE STRESS

Let us determine the design criterion corresponding to Eq. (4) in the case of uniaxial Gaussian stress :

$$\tilde{\sigma}_x(t) = \sigma_0 + \sigma_x \sin(\omega t + \alpha) \tag{6}$$

with the random amplitude σ_x and random phase angle α. As to the stress amplitude it follows Rayleigh distribution [3] :

$$F(\sigma_x) = 1 - \exp\left(-\frac{\sigma_x^2}{2s_x^2}\right) \tag{7}$$

where : s_x is the standard deviation of the stress amplitude.

In terms of ensemble averages, the counterpart of the criterion (4) reads :

$$\frac{N_d}{K\left(1 - \frac{\sigma_0}{R_e}\right)^m} E\{\sigma_x^m\} < 1 \tag{8}$$

where : $E\{\cdot\}$ denotes the expected value. In the considered case :

$$E\{\sigma_x\} = (0.5\pi)^{1/2} s_x \tag{9}$$

$$E\{\sigma_x^m\} = 2^{m/2}\Gamma\left(1+\frac{m}{2}\right)s_x^m \tag{10}$$

where : Γ is the gamma function.
So, the criterion (8) becomes :

$$\frac{2^{m/2}N_d}{K\left(1-\frac{\sigma_0}{R_e}\right)^m}\Gamma\left(1+\frac{m}{2}\right)s_x^m < 1 \tag{11}$$

for :

$$Z_{rc}\left(1-\frac{\sigma_0}{R_e}\right) < (0.5\pi)^{1/2}s_x \le L\left(1-\frac{\sigma_0}{R_e}\right)$$

FATIGUE-CRITICAL STRESS AMPLITUDE AND PROBABILITY OF FATIGUE FAILURE UNDER STATIONARY RANDOM-AMPLITUDE STRESS

Eqs (9) and (11) yield :

$$\frac{N_d\Gamma\left(1+\frac{m}{2}\right)[E\{\sigma_x\}]^m}{(0.25\pi)^{m/2}\left(1-\frac{\sigma_0}{R_e}\right)^m K} < 1 \tag{12}$$

Hence the expected value of the fatigue-critical amplitude of the stress (6) can be estimated as :

$$\sigma_{cr} = (0.25\pi)^{1/2}\left(1-\frac{\sigma_0}{R_e}\right)\left[\frac{K}{N_d\Gamma\left(1+\frac{m}{2}\right)}\right]^{1/m} \tag{13}$$

With the respect to the distribution function (7), the probability, P_{cr}, of exceedance of the fatigue-critical stress amplitude is given by :

$$P_{cr} = P\{\sigma_x \ge \sigma_{cr}\} = \exp\left(-\frac{\sigma_{cr}^2}{2s_x^2}\right) \tag{14}$$

From Eqs (13) and (14) one obtains :

$$P_{cr} = \exp\left\{-\frac{0.25\pi}{2s_x^2}\left(1-\frac{\sigma_0}{R_e}\right)^2\left[\frac{K}{N_d\Gamma\left(1+\frac{m}{2}\right)}\right]^{2/m}\right\} \tag{15}$$

Now, the task is to determine the relation between P_{cr} and the probability, P_f, of fatigue failure under the stress (6). According to the Palmgren-Miner rule [1, 2] the increment of fatigue damage, caused by N_d stress cycles of constant amplitude is equal to the ratio N_d/N where N is the cycle number to cause failure. Referring to the stress (6) the expected cycle number to failure can be estimated by means of Eq. (12) as :

$$N = \frac{(0.25\pi)^{m/2}\left(1-\frac{\sigma_0}{R_e}\right)^m K}{\Gamma\left(1+\frac{m}{2}\right)[E\{\sigma_x\}]^m} \tag{16}$$

Hence the expected value, D, of the fatigue damage after N_d cycles is :

$$D = \frac{N_d\Gamma\left(1+\frac{m}{2}\right)[E\{\sigma_x\}]^m}{(0.25\pi)^{m/2}\left(1-\frac{\sigma_0}{R_e}\right)^m K} \tag{17}$$

and the probability of fatigue failure :

$$P_f = P\{D \ge 1\} \tag{18}$$

becomes :

$$P_f = P\left\{\sigma_x \ge (0.25\pi)^{1/2}\left(1-\frac{\sigma_0}{R_e}\right)\left[\frac{K}{N_d\Gamma\left(1+\frac{m}{2}\right)}\right]^{1/m}\right\} = P[\sigma_x \ge \sigma_{cr}] \tag{19}$$

Hereby the following has been proved : **In the high-cycle regime the probability of fatigue failure under random--amplitude stress is equal to the probability of exceedance of the fatigue-critical stress amplitude**.

EXAMPLE

Let us consider a stationary random stress :

$$\tilde{\sigma}_x(t) = \sigma_0 + \tilde{\sigma}_r(t) \tag{20}$$

where : σ_0 is the mean value of the stress $\tilde{\sigma}_x(t)$ and $\tilde{\sigma}_r(t)$ is the stationary (in the wide sense) stochastic process of zero mean value and known power spectral density $S(\omega)$. The suggestion is to model the stress $\tilde{\sigma}_x(t)$ by the equivalent stress $\tilde{\sigma}_e(t)$ in the form of a periodic (in the mean-square sense [4]) Gaussian process :

$$\begin{aligned}\tilde{\sigma}_e(t) &= \sigma_e + a\sin(\omega_e t + \varphi) = \\ &= \sigma_e + a_1\exp(j\omega_e t) + a_2\exp(-j\omega_e t)\end{aligned} \tag{21}$$

where :

σ_e – the mean value of the stress $\tilde{\sigma}_e(t)$
ω_e – the circular frequency of the equivalent stress
a – the random amplitude of Rayleigh distribution
φ – the random phase and :

$$a_1 = \frac{a}{2j}\exp(j\varphi) \quad , \quad a_2 = a_1^*$$

$$E\{a_1\} = E\{a_2\} = E\{a_1 a_2^*\} = E\{a_1^* a_2\} = 0$$

$(\cdot)^*$ – complex conjugate
j – imaginary unity.

Following the approach based on the theory of energy transformation systems [5] and presented in [6], the equivalence conditions are :

$$\begin{aligned}E\{\tilde{\sigma}_e(t)\} &= E\{\tilde{\sigma}_x(t)\} \\ C_{\tilde{\sigma}_e}(\tau) &= C_{\tilde{\sigma}_x}(\tau) \\ C_{\dot{\tilde{\sigma}}_e}(\tau) &= C_{\dot{\sigma}_x}(\tau)\end{aligned} \tag{22}$$

where : C stands for the autocorrelation function, τ is the time interval, and dot denotes the time derivative. The results of calculation are as follows :

$$\begin{aligned}\sigma_e &= \sigma_0 \\ s_e &= \left[\int_{-\omega}^{\infty} S(\omega)d\omega\right]^{1/2} \\ \omega_e &= \left[\frac{\int_{-\infty}^{\infty}\omega^2 S(\omega)d\omega}{\int_{-\omega}^{\infty} S(\omega)d\omega}\right]^{1/2}\end{aligned} \tag{23}$$

where : s_e is the standard deviation of the equivalent stress amplitude.

By analogy with the stress (6) and Eq. (13), the expected value of the fatigue-critical amplitude of the equivalent stress is as follows :

$$a_{cr} = (0.25\pi)^{1/2}\left(1-\frac{\sigma_0}{R_e}\right)\left[\frac{2\pi K}{\omega_e T_d \Gamma\left(1+\frac{m}{2}\right)}\right]^{1/m} \quad (24)$$

where : T_d is the required design life (in seconds).

Consequently, when the following condition is met :

$$Z_{rc}\left(1-\frac{\sigma_0}{R_e}\right) < (0.5\pi)^{1/2} s_e \le L\left(1-\frac{\sigma_0}{R_e}\right) \quad (25)$$

the probability of fatigue failure during the time T_d can be estimated as :

$$P_f = P\{a \ge a_{cr}\} = \exp\left(-\frac{a_{cr}^2}{2s_e^2}\right) \quad (26)$$

If :

$$(0.5\pi)^{1/2} s_e > L\left(1-\frac{\sigma_0}{R_e}\right) \quad (27)$$

the low-cycle fatigue failure may occur.

In the case of :

$$(0.5\pi)^{1/2} s_e \le Z_{rc}\left(1-\frac{\sigma_0}{R_e}\right) \quad (28)$$

an infinite fatigue life may be expected.

Its probability is considered in [6].

CONCLUSIONS

- The deterministic and probabilistic fatigue-critical amplitudes of uniaxial asymmetric stresses are defined as those which lead to high-cycle fatigue failure during the required design life.
- It is found that the probability of fatigue failure under random-amplitude stress is equal to the probability of exceedance of the fatigue-critical stress amplitude.
- It is shown how the probability of fatigue failure under stationary random stress of known power spectral density can be estimated by means of the fatigue-critical amplitude of the equivalent random-amplitude stress.

NOMENCLATURE

a – amplitude of the equivalent stress
a_{cr} – fatigue-critical amplitude of the equivalent stress
C – autocorrelation function
D – fatigue damage accumulated during the required design life
$E\{\cdot\}$ – expected value
F – distribution function
j – imaginary unity
K – fatigue strength coefficient
L – maximum stress amplitude satisfying equation of the S-N curve (above which low-cycle fatigue is possible)
m – fatigue strength exponent
N – number of stress cycles to cause fatigue failure
N_d – required cycle number
P – probability
P_{cr} – probability of exceedance of the fatigue-critical stress amplitude
P_f – probability of fatigue failure
R_e – tensile yield strength
S – power spectral density
s_e – standard deviation of the equivalent stress amplitude
s_x – standard deviation of the stress amplitude
t – time
Z_{rc} – fatigue limit under fully reversed tension-compression
α – phase angle of the stress (6)
Γ – gamma function
σ – amplitude of the fully reversed stress
$\tilde{\sigma}$ – asymmetric stress
σ_a – amplitude of the stress (1)
σ_{cr} – fatigue-critical stress amplitude
σ_e – equivalent mean stress
$\tilde{\sigma}_e$ – equivalent stress
σ_0 – mean stress
$\tilde{\sigma}_r$ – stationary random stress of zero mean value
σ_x – amplitude of the stress (6)
$\tilde{\sigma}_x$ – asymmetric random-amplitude stress, asymmetric random stress
τ – time interval
φ – phase angle of the equivalent stress
ω – circular frequency
ω_e – circular frequency of the equivalent stress
$(\,)^*$ – complex conjugate

BIBLIOGRAPHY

1. Kocańda S., Szala J.: *Fundamentals of fatigue calculations* (in Polish). PWN (State Scientific Publishing House). Warszawa. 1997
2. Almar-Naess A. (Ed.): *Fatigue handbook. Offshore steel structures*. Tapir Publishers. Trondheim. 1985
3. Pacut A.: *Probability theory. Probabilistic modeling in technology* (in Polish). WNT (Scientific - Technical Publishing House). Warszawa. 1985
4. Preumont A.: *Vibrations aléatoires et analyse spectrale*. Lausanne: Presses Polytechniques et Universitaires Romandes, CH-1015. 1990
5. Cempel C.: *Theory of energy transformation systems and their application in diagnostic of operating systems*. Applied Math. and Computer Sciences, No 2/1993
6. Kolenda J.: *On fatigue safety of metallic elements under static and dynamic loads*. Gdańsk University of Technology Publishers. 2004

CONTACT WITH THE AUTHOR
Prof. Janusz Kolenda
Faculty of Ocean Engineering
and Ship Technology,
Gdańsk University of Technology
Narutowicza 11/12
80-952 Gdańsk, POLAND
e-mail : sek7oce@pg.gda.pl

Main building of the Faculty of Ocean Engineering and Ship Technology, Gdańsk University of Technology

Application of movable approximation and wavelet decomposition to smoothing-out procedure of ship engine indicator diagrams

Stanisław Polanowski
Polish Naval University

ABSTRACT

In this paper - on the basis of indicator diagram processing taken as an example - were shown possibilities of the smoothing-out and decomposing of run disturbances with the use of the movable multiple approximation based on the least squares criterion. The notion was defined of movable approximating object and constraints used to form approximation features. It was demonstrated that the multiple approximation can be used to decompose disturbances out of an analyzed run. The obtained smoothing-out results were compared with those obtained from full-interval approximation of runs by means of splines as well as wavelet decomposition with using various wavelets, Wavelet Explorer and Mathematica software. Smoothing-out quality was assessed by comparing runs of first derivatives which play crucial role in the advanced processing of indicator diagrams.

Keywords : smoothing-out the runs, least squares method, full-interval approximation, movable approximation, decomposition of disturbances, cut constraints, glued constraints, riveted constraints, broken constraints, weighting factors, wavelet decomposition.

INTRODUCTION

Advanced acquisition of diagnostic information from indicator diagrams is associated mainly with determination of first derivative necessary for determining heat emission characteristics. For certain purposes also determination of second derivative and even third one may be necessary.

With determination of derivatives the necessity of smoothing-out indicator diagrams is associated. A. Ralston has defined the notion of smoothing-out in such a way that if an approximation maintains information on function resulting from measurements and fades away disturbances then it is said that it smooths out (levels) measurement data [8].

In this work - to compare effectiveness of various approximation methods – the indicator diagram (shown in Fig. 1, 2) was used; it was obtained from measurements performed in a cylinder of Sulzer 6AL20/24 ship medium-speed engine for the loading parameters : n = 750 rpm, p_i = 1.8 MPa. Beginning from the instant of ignition up to the end of combustion process, on the run of the pressure **p** can be observed pressure oscillations of large values generated by a short measuring channel (10 mm long) between the combustion chamber and gauge membrane. The indicator diagram of **p** was recorded with 0.1°owk angular resolution and 12 bit amplitude resolution.

FULL-INTERVAL APPROXIMATION OF RUNS BY USING THE LEAST SQUARES METHOD

Measurement data processing is aimed at assessing real values of measured quantities or searching for functional relationships whose mathematical model is either known or searched for. To this end, is usually applied the least squares method whose essence consists in the determination of minimum of the following functional :

$$\mathrm{MIN}(S) = \mathrm{MIN}\left[\sum_{1}^{N} (\tilde{y}_i - \hat{y}_i)^2\right] \tag{1}$$

where :

MIN – operator of minimum value
N – number of elements of a measurement set
S – sum of squares of deviations
$\tilde{y}_i$ – measured values
$\hat{y}_i$ – approximated values.

Relations between measured, real and approximated values are determined by the equality :

$$\tilde{y}_i = y_i + \varepsilon_{Ri} = \hat{y}_i + \varepsilon_a = \hat{y}_i + \varepsilon_{Mi} + \varepsilon_{Ri} \qquad (2)$$

where :

y_i – real value of measured quantity
ε_{Ri} – measuring error
ε_a – approximating error
ε_{Mi} – modelling error.

If to find an adequate mathematical model of measured quantity run is not possible then it is usually approximated by means of a linear combination of selected elementary functions. As an orthogonal basis power polynomials or trigonometric ones are most often used; the latter - in the cases where periodic runs are analyzed. Sometimes non-linear models may be linearized or their parameters determined by using the theory of experiments.

The known difficulties in performing the full-interval approximation with the use of power polynomials are tried sometimes to be overcome by using splines.

A drawback of such functions is their high suceptibility to generate oscillations appearing especially in runs of derivatives derived from measurement data [6] (see e.g. Fig.1).

As it results from comparison of the runs of the derivative p'_{60} and p'_{F3}, the symptoms S_{CK} and S_R have been smoothed out for the number of nodes equal to 60. For the number of nodes equal to 180, the symptoms S_{CK} and S_R appeared - but with significant oscillations - on the run of p'_{180}.

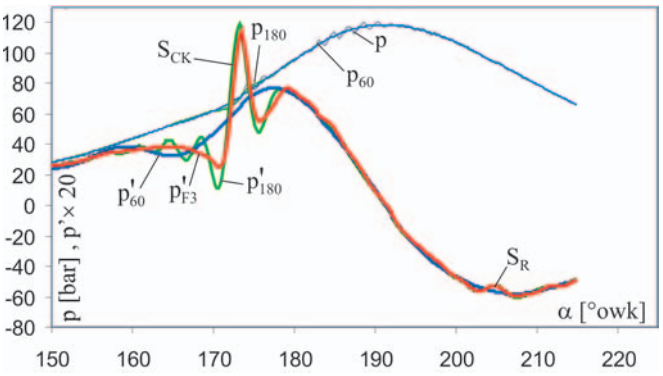

*Fig. 1. Comparison of smoothing-out quality of the indicator diagram **p** by means of glued 5th order polynomials and movable approximation with the use of the object F3 (Fig.2). **Notation** : p_{60}, p_{180}, p'_{60}, p'_{180} – runs and their derivatives obtained by approximating the run **p** with the use of the glued 5th order polynomial for the number of nodes given by their respective indices, p'_{F3} – first derivative derived from the run **p** by means of the movable approximation by making use of the object F3, S_{CK} – kinetic combustion symptom, S_R – fuel re-injection symptom, α - crankshaft rotation angle [°owk]*

The oscillations are increasing along with constraint number increasing. As proved, no such number of nodes exists that the first derivative run obtained for which, could be considered matching the run p'_{F3}.

Worth mentioning that the smoothing-out quality of pressure run itself in the form of the runs p'_{60}, p'_{180} can be considered sufficient for certain purposes despite that the quality of determination of first and higher derivatives is insufficient. In the case of rather non-dynamical runs (such as e.g. those of pure compression, sinusoid, etc), by applying the full-interval approximation with splines a sufficient smoothing-out quality can be obtained also in the aspect of determining derivatives, but usually can not in the case of the indicator diagrams of combustion process.

SMOOTHING-OUT THE RUNS AND DECOMPOSITION OF DISTURBANCES BY MEANS OF THE MOVABLE MULTIPLE APPROXIMATION METHOD

An obvious way for diminishing the errors occurring at application of the full-interval approximation method is to split a given data interval into smaller ones, that leads to the movable approximation process.

The movable approximation consists in determining – in every point **n** of measurement series – a value approximated over a movable approximation interval of a given width. The point **n** of movable approximation is called the control point.

If the minimum value of sum of squares of deviations is assumed the approximation criterion then for P-th step (repetition) of approximation the criterion can be written as follows :

$$\mathrm{MIN}(S_{Pn}) = \mathrm{MIN}\left[\sum_{i=n-k_{lP}}^{i=n-k_{rP}} (\hat{y}_{(P-1)i} - \hat{y}_{Pi})^2\right] \qquad (3)$$

where :

MIN – operator of searching for minimum
S_{Pn} – sum of squares of deviations in the point n for P-th step of approximation
$\hat{y}_P$ – values obtained from approximation for its step P
$\hat{y}_{0i} = \tilde{y}_i$ – measured values
k_{lP} , k_{rP} – parameters of the left and right end of interval of approximation for its step P.

Usually the central intervals of approximation, i.e. $k_{lP} = k_{rP} = k$, are applied.

The simplest example of the movable approximation is the movable average method. A natural generalization of the movable average method has been the algorithms of movable least squares approximation with the use of higher-order power polynomials, elaborated by Savitzky and Golay [9]. In this work the algorithms of movable approximation with power polynomials elaborated by this author [2, 3, 5], were applied; they were next extended by applying the approximating objects with constraints [4, 7].

In Fig.2 are shown results of the multiple approximation of the indicator diagram **p** with the use of the approximating object F3 being a power polynomial of 3rd order. To obtain a sufficiently smooth run of the first derivative p'_{F3} the approximation by using

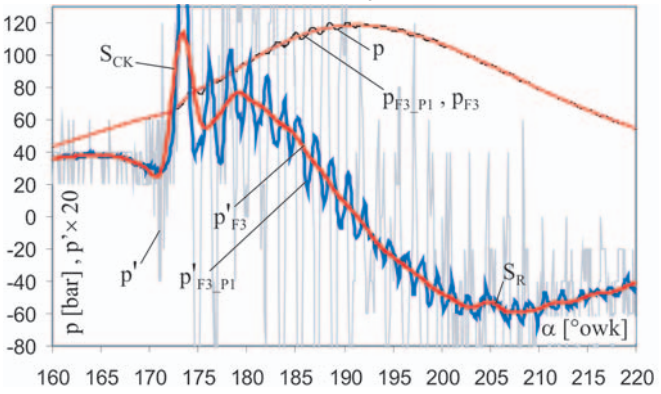

*Fig. 2. Illustration of smoothing-out effectiveness of the indicator diagram **p** with the use of the approximating object F3. **Notation** : F3 – 3rd order power polynomial - central object, k = 16, P = 5; p' – first derivative determined as linear increments of the run p; p_{F3_P1} , p'_{F3_P1} – the smoothed-out run and first derivative after 1st step of approximation; p_{F3} , p'_{F3} – the smoothed-out run and first derivative after 5th step of approximation ($p_{F3} = p_{F3\_P5}$, $p'_{F3} = p'_{F3\_P5}$); S_{CK} – kinetic combustion symptom, S_R – fuel re- injection symptom.*

the object F3 was performed five times for the same value of k = 16. The run of the first derivative p' (Fig.2), determined as linear increments of the curve **p**, illustrates the scale of difficulty which is to be overcome to obtain a smooth derivative run not loaded by dynamic errors, such as the run p'_{F3} (Fig.2) assumed in this work for the quality assessment of smoothing-out the run **p** with the use of other approximating objects and methods. To this end, in Fig.2 were distinguished the peaks (symptoms) S_{CK} , S_R ; on their runs conclusions as to dynamic features of the considered approximation method, can be based.

The multiple approximation method can be also applied to decompose disturbances. The total deviation of n-th sample of measurement series after performance of P-th approximation, is equal to :

$$D\hat{y}_{Pn} = \tilde{y}_n - \hat{y}_{Pn} \tag{4}$$

The deviation can be presented in the form of component deviations for distinguished steps of approximation. If the steps 1, g, u, P are distinguished this is equivalent to four decomposition levels at which four runs of deviations which satisfy the below given equation, can be obtained :

$$Dy_{Pn} = Dy_{01n} + Dy_{1gn} + Dy_{gun} + Dy_{uPn} \tag{5}$$

Other number of decomposition levels (steps) can be also assumed or to perform decomposition of disturbances after ending the approximation. Hence, auxiliary steps and main ones of the approximation have been distinguished. In order to achieve final smoothing-out to perform the auxiliary steps is not necessary.

Selection of decomposition parameters as well as assessment of its results depends on expectations, i.e. on knowledge of a physical character of achieved results - otherwise they may be of no subject-matter merit.

The high-frequency disturbances Dp_{F01}, Dp_{F12} of the run **p** (Fig. 2) determined in two auxiliary steps of the approximation with the use of the approximating objects F3a and F3b, are shown in Fig.3.

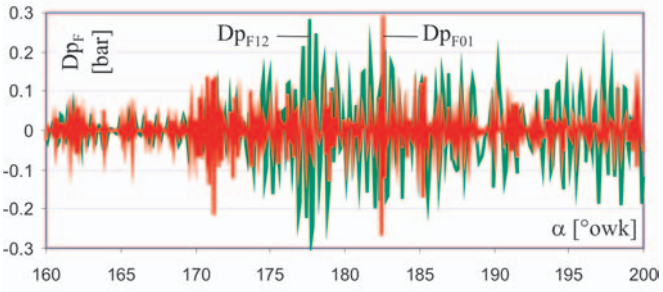

Fig. 3. *The disturbances Dp_{F01} , Dp_{F12} separated in two auxiliary steps of the approximation of the run **p** (Fig.2) with the use of the objects F3a and F3b.* ***Notation*** *: F3a – 3rd order power polynomial, k = 2; F3b – 3rd order power polynomial, k = 4; $Dp_{F01} = p - p_{F3a}$, $Dp_{F12} = p - p_{F3b}$; where: p_{F3a} – the run determined from the run **p** with the use of the object F3a, p_{F3b} – the run determined from the run **p** with the use of the object F3b.*

The disturbances Dp_{F01} , Dp_{F12} are composed of A/D processing errors, disturbances within measuring lines, measuring gauge errors and high-frequency components involved by gas passages.

The disturbances separated from the run **p** in five main steps of the approximation with the use of the object F3 are shown in Fig. 4.

The runs of disturbances shown in Fig. 4 result mainly from interaction of the gas channel between the cylinder working space and gauge membrane, as well as they may contain a part of useful signal due to inadequacy of the approximating object's model.

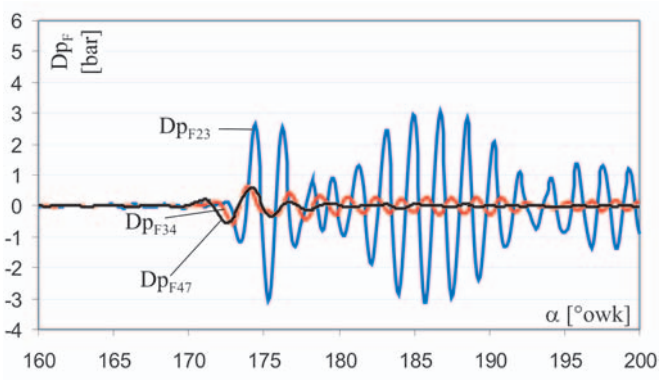

Fig. 4. *The disturbances Dp determined in five main steps of smoothing-out the indicator diagram **p** by using the object F3.* ***Notation*** *: $Dp_{F23} = p_{F3\_P1} - p_{F3b}$, $Dp_{F34} = p_{F3\_P2} - p_{F3\_P1}$, $Dp_{F47} = p_{F3\_P5} - p_{F3\_P2}$, where : p_{F3b} (Fig. 3), p_{F3_P1} ,…, p_{F3_P5} – the runs determined in result of approximation of the run **p** by using the object F3 (Fig.2).*

The run of the deviations Dp_{F47} can be represented by their three components [1]. The deviations were summed – up with taking into account their similarity.

In the smoothing-out process of the run **p** the objects F3a and F3b were not used for determining the derivative p'_{F3} (Fig.2). However if to include the objects into the smoothing-out process of the run **p** then in the example in question the first derivative determined this way will be almost identical - the differences will not exceed ±0.01% of the maximum value of p'_{F3} . Number of possible decompositions of deviations of measured run from that smoothed-out is very high for the example in question but such decompositions may be of no physical sense.

MOVABLE APPROXIMATING OBJECTS WITH CONSTRAINTS

The power polynomials free of constraints applied in Savitzky-Golay filters not always ensure a sufficient quality of approximation. Quality of approximation and decomposition of runs can be formed by modifying the approximating functions by applying constraints onto values of left-hand and right-hand derivatives of the functions in the points (nodes) q_v (Fig.5).

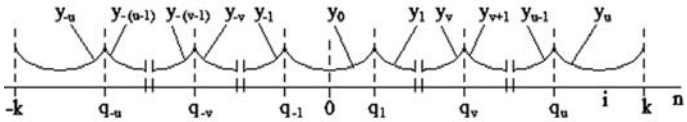

Fig. 5. *Schematic diagram of the central approximating object.* ***Notation*** *: y_v – approximating functions, {v = -u (1) u}; q_v – node coordinates, {v = - u (1) u}; i – approximating object axis, i = 0 – control point; n – axis of measurement series, n =1(1)N; k – width parameter of approximating object interval.*

It was assumed that approximating object is central one if its control point is located in the mid-point of the approximating object. Approximating object is symmetrical if the symmetry of nodes, constraints and kinds of functions (coefficients) regarding the mid-point of the object, takes place.

For the sake of easiness of formulating mathematical description of approximating object, the axis of arguments and that of approximating object was introduced where the control point coordinate is i = 0 for every successive **n**. Usually the control point is located in the mid - point of the approximation interval of the approximating object (Fig.5). If a node is placed in the control point then q_0 , but not y_0 , will appear in the object's model, that results from the assumed indexing principle.

Smoothing-out features of approximating object can be formed by setting-up its structure and values of its parameters including :

- type of approximating functions
- number of nodes and constraints
- kind of constraints: cut (spline), glued, riveted, broken ones
- either symmetry or asymmetry of function coefficients, location of control point, coordinates of nodes and their parameters, type of base functions.

The cut constraint takes place in a given node q_v of approximating object if at least one of the derivatives of approximating function is cut (unconstrained) in that node :

$$y_{v-1}^{(m)}(q_v) \,\mathrm{W}_m\, y_v^{(m)}(q_v) \;,\; y_{v-1}(q_v) = y_v(q_v) \tag{6}$$

where :

m – order of derivative

W_m – symbol of cutting (non-constraining) of m-th derivative.

Such constraints are used to build splines. Obviously, appearance of even a single constraint of the kind in a given node produces an indeterminate break of function (depending on disturbances).

The glued constraint in a given node q_v takes place if the following relationships occur :

$$y_{v-1} \neq y_v \;,\; y_{v-1}^{(m)}(q_v) = y_v^{(m)}(q_v)$$
$$y_{v-1}(q_v) = y_v(q_v) \tag{7}$$

As it results from that definition the functions to the right and to the left from the node q_v are of different types.

The broken constraint consists in setting the breaking coefficient $w_{q_v}^{(m)} \neq 1$ for a given m-order derivative in a given node q_v , that is equivalent to imposing a definite discontinuity of the derivative in the node in question. Values of approximating function in nodes are assumed continuous. By using the notation from Fig.5 the above given definition can be expressed as follows :

$$y_{q_v}^{(m)}(q_v) = w_{q_v}^{(m)} y_{q_v-1}^{(m)}(q_v)$$
$$y_{q_v}^{(0)}(q_v) = y_{q_v-1}^{(0)}(q_v) \;,\; w_{q_v}^{(m)} \neq 1 \tag{8}$$

The broken constraints differ from the cut ones applied to spline functions by that they are assumed determined ones.

The spline constraints are free (undetermined), that results from cutting the selected derivatives. The simplest broken object is a broken line built of straight segments.

The riveted constraints of two sections of approximating object's function occurs when the overlapping of intervals of left and right approximating functions takes place, that can be expressed as follows :

$$r_v \neq l_{v+1} \tag{9}$$

as well as when equality of the function or one of its derivatives occurs even in a single node.

In Fig.6 is shown an example of a simple riveted approximating object of three nodes in which values of the function are riveted.

The features of the above defined approximating objects are illustrated by a few examples of their application to smoothing-out the runs [1, 7].

Approximating object features can be also formed by inserting weights (weighting functions) into approximation equations. The weighting methods are used in statistical data analysis, especially in the case of smoothing-out small data sets. The weights constitute a kind of constraints imposed upon function values.

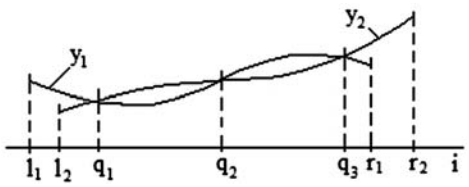

Fig. 6. Schematic diagram of the approximating object riveted in three points : $y_1(q_1) = y_2(q_1)$, $y_1(q_2) = y_2(q_2)$, $y_1(q_3) = y_2(q_3)$; for the central object the following is valid: $r_2 = -l_1$, $r_1 = -l_2$, $q_3 = -q_1$, $q_2 = 0$.

Staś [10], basing on a reference, gave an example of smoothing-out object which could be effective in the case of smoothing-out the indicator diagram. His formula for the smoothing-out object in question can be expressed – after formal transformation – as follows :

$$\hat{y}_i = \sum_{i=-k}^{k} w_i \tilde{y}_i \tag{10}$$

where the weights $\mathbf{w}_i$ are determined from the formula :

$$w_i = \left[\sum_{i=-k}^{k}\binom{2k}{i+k}\right]^{-1}\binom{2k}{i+k} \;,\; \sum_{1=-k}^{k} w_i = 1 \tag{11}$$

where :

k – interval width parameter of approximating object in question.

As demonstrated, multiple approximation of the run **p** by using the object F0w with weights has not led to any better result of smoothing-out as compared with that obtained by means of the simple movable average (object F0) (Fig.7).

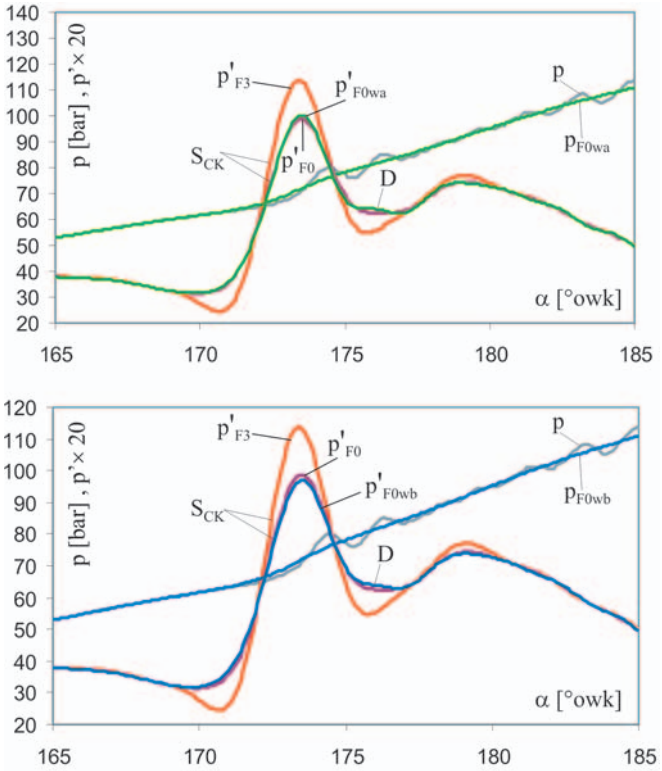

Fig. 7. *Comparison of smoothing-out quality of the run **p** by using the movable average (object F0) and that obtained by means of the movable weighted average (object F0w). Parameters of the smoothing-out objects: **F0**: k = 8, P = 4; **F0wa**: k = 8, P = 25; **F0wb**: k = 32, P = 7; p_{F0wa} , p'_{F0wa} – the smoothed-out run and its first derivative determined by means of the object F0wa, p_{F0wb} , p'_{F0wb} – the smoothed-out run and its first derivative determined by means of the object F0wb, D – deformation .*

As seen in Fig.7, in the case of application of the object F0wa, as many as P = 25 smoothing-out steps are necessary

to obtain the result comparable with that achieved by using the object F0 (P = 4) which is the simple movable average. Additionally, the deformation D appeared on the derivative p'_{FOwa}. The increasing of k value up to k = 32 resulted in the decreasing number of smoothing-out steps P = 7, but it did not provide any practical benefits as compared with the results of application of the movable average. In both the cases the derivatives significantly differ from the reference run p'_{F3} obtained by using the object F3.

However the application of weighting functions changes smoothing-out features of approximating object and in certain cases their application may be justified.

DECOMPOSITION OF RUNS BY MEANS OF WAVELET FILTERS

In technical diagnostics are observed many attempts to apply wavelet analysis for separating – from measured runs – – the signals containing diagnostic information. The pressure run **p** was subjected to decomposition by using six known wavelet filters (offered in the Wavelet Explorer package in cooperation with Mathematica software) for various parameters of the filters [11].

In Fig.8 are shown the results obtained by using Daubechies and Shannon filters of the parameters given in their indices.

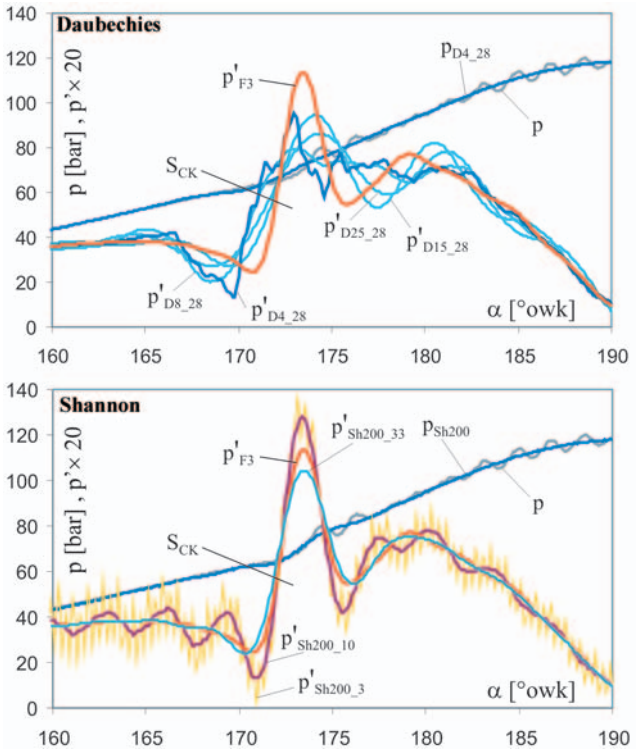

Fig. 8. *Comparison of the results of smoothing-out the indicator diagram* ***p*** *by means of wavelet filters of two kinds with those obtained by using the object F3.* ***Notation*** *: the indices of p and p': **D** – Daubechies filter, **Sh** - Shannon filter; numerical values of the indices, e.g. 4_28, stand for parameters of a given filter acc. Wavelet – Explorer description; for p'_{Sh200_3}, p'_{Sh200_10}, p'_{Sh200_33} the index values_3; _10; _33 stand for the values of the parameter k of the smoothing-out object (3rd order power polynomial) .*

As seen in Fig. 8 the first derivatives achieved from the runs smoothed-out by using the filters are impermissibly distorted as compared with the run p'_{F3} obtained by using the object F3. In the case of Shannon filter the additional smoothing-out by means of the movable approximation method made it possible to obtain the run p'_{Sh200_33} which is very similar to the run p'_{F3}. In the case of the remaining filters the additional smoothing-out can not provide any improvement because of subsequent loss of information. The first derivative deformations analogous to those in the case of Daubechies filter, were obtained by using also other wavelet filters, such as e.g. : Meyer's, Least Asymmetric, Spline and Coiflet filter [11]. It should be stressed that Shannon filter is deemed one of the worst. However in this case it was the only one which made it possible – after application of additional smoothing-out procedure – to obtain sufficiently correct results. The wavelet decomposition of runs provides also disturbance runs in the form of the so-called details. In Fig.9 are shown the high-frequency details Dp_{Sp4} , Dp_{Sp3} obtained for two first steps of decomposition by means of the filter Sp3_50 (Fig.8).

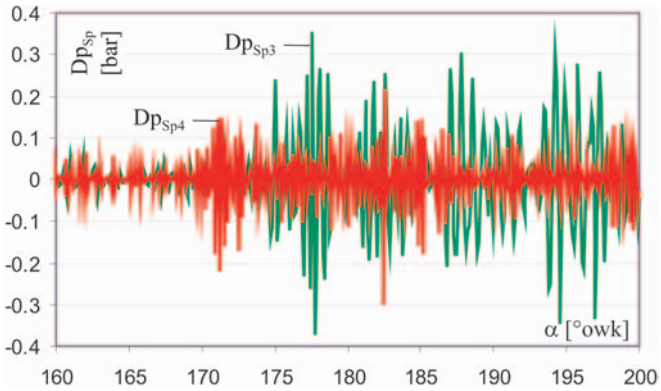

Fig. 9. *Runs of the high-frequency details (deviations) Dp_{Sp4} , Dp_{Sp3} separated in result of decomposition of the run* ***p*** *by using the filter Sp3_50 (Fig.8) .*

Comparing the runs Dp_{Sp4}, Dp_{Sp3} (Fig.9) with the runs Dp_{F01}, Dp_{F12} (Fig.3) one can postulate that they are similar (convergent) to each other. Degree of convergence of the runs can be assessed by performing direct comparison, correlation or coherence analysis.

In the case of low-frequency deviations (Fig.10) a noticeable convergence of the runs Dp_{Sp1} and Dp_{Sp2} with the runs Dp_{F23} (Fig.4) can be observed; however the level of their differences can not be considered negligible.

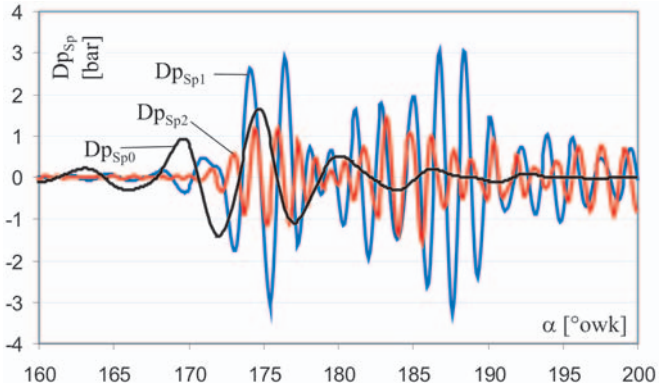

Fig.10. *Runs of the low-frequency details (deviations) Dp_{Sp0} , Dp_{Sp1} and Dp_{Sp2} separated in result of decomposition of the run* ***p*** *by using the filter Sp3_50 (Fig. 8) .*

Analyzing the runs Dp_{F23}-Dp_{F47} (Fig. 4) one can observed that in the applied display scale the waving on the runs within the coordinate interval up to the angle α = 170°owk, or even to 172°owk, are not visible. However in the case of the run Dp_{Sp0} (Fig. 10) a significant waving can be observed beginning already from the angle α = 160°owk. The run Dp_{Sp0} has not any equivalent among the runs presented in Fig. 4. Beginning from the angle α = 168°owk, a significant waving is also visible on the run Dp_{Sp1} (Fig. 10), which deforms the first derivative run p'_{Sp3_50} to an impermissible degree (Fig. 8).

Such phenomena were observed in analyzing a number of other runs including those much less disturbed, and in every case negative result was obtained of smoothing-out process for

determining first derivative, except the case of the application of Shannon filter connected with final smoothing-out operation. The problems may serve as subjects of separate research.

CONCLUSIONS

- By applying the multiple movable approximation of runs by using objects of appropriately selected features to obtain a demanded degree of smoothing-out the run and to perform decomposition of distortions, is possible.
- To form features of approximating objects can be used : cut, glued, broken or riveted constraints as well as weights. The features can be formed by choosing : kind of base functions, width of object's interval, number and kind of constraints, number and location of nodes. Multiplicity of approximation repetitions (number of steps) influences smoothing-out results specially.
- The full-interval approximation of runs by using spline functions may lead to significant errors in the form of generation of waving which does not exist really.
- The decomposition (filtration) by means of wavelets may be also loaded by significant errors both as to the smoothed-out run and the obtained details (deviations). It does not contradict the usefulness of the method for e.g. image compression where the disturbance level involved by wavelet filters may be insignificant. Applying the method for filtration of diagnostic signals in engineering one should be careful in accepting the obtained results especially if their confirmation by any other method is not performed.

NOMENCLATURE

D – run distortion,
F3 – movable approximating object : 3rd order polynomial, k = 16, P = 5
i – axis of arguments of an approximating object
k – width parameter of approximation interval of central object
m – derivative order
n – numerical axis of measurement series, n = 1(1)N
P – number of steps (passages) of approximation
p – run of cylinder pressure (indicator diagram)
p' – first derivative of the pressure p
p'_{F3} – first derivative of the pressure p determined with the use of the object F3
q, q_v – node coordinates of the approximating object, {v = - u (1) u}
S_{CK} – kinetic combustion symptom
S_R – re-injection symptom
$\hat{y}$ – approximating function
$\tilde{y} = y$ – measurement series
y_v – approximating function, {v = -u (1) u}
$y_v^{(m)}$ – *m-th* derivative of the function y_v
α – crankshaft rotation angle
°owk – degree of crankshaft rotation angle

BIBLIOGRAPHY

1. Polanowski S.: *Analysis of measurement data with application of movable approximating objects* (in Polish). Scientific Bulletins of Polish Naval University (Zeszyty Naukowe AMW), no. 2 (157). Gdynia, 2004
2. Polanowski S.: *Follow-up approximation of combustion pressure run and generation of derivatives and integrals* (in Polish). Journal of Internal Combustion Engines KONES, 1996
3. Polanowski S.: *The Following Approximation of Cylinder Pressure Run and Generation of Derivatives and Integrals.* Journal of Polish CIMAC. 1996
4. Polanowski S.: *Smoothing and decomposition of disturbances of indicator diagrams with applications of the moving approximating objects with broken bonds*. Vol. 12, Journal of Internal Combustion Engines – KONES. 2005
5. Polanowski S.: *Fast processing of indicator diagram for control and steering purposes* (in Polish). Proc. 3rd Scientific Symposium EKODIESEL'96. Warszawa, 1996
6. Polanowski S., Zellma M.: *The peak value determination of cylinder pressure rate with the basic splines or follow-up approximation*. Proc. of the Conference KONES'97
7. Polanowski. S.: *The processing of indicator diagrams with the use of the moving approximating objects*. Combustion Engines. No 1/2005.
8. Ralston A. : *Introduction to numerical analysis* (in Polish). Scientific Technical Publishing House (PWN). Warszawa, 1983
9. Savitzky A., Golay M.J.E.: *Smoothing and Differentiation of Data by Simplified Least Squares Procedures*. Vol. 36, Analytical Chemistry 1964
10. Staś M. J.: *Preparation of diesel engine indicator diagrams for cycle calculations*. Proc. of the Conference KONES'99.
11. Wysocki H., Polanowski S.: *Wavelet decomposition of ship engine indicator diagram by means of Wavelet Explorer software* (in Polish). Scientific Bulletins of Polish Naval University (Zeszyty Naukowe AMW)No. 1(160). Gdynia, 2005

CONTACT WITH THE AUTHOR
Stanisław Polanowski, D.Sc., Eng.
Mechanic-Electric Faculty,
Polish Naval University
Śmidowicza 69
81-103 Gdynia, POLAND
e-mail : SPolanowski@o2.pl

Miscellanea

Days of Engineering

On 23-25 November 2006, 37th Days of Engineering was held on the occasion of 60th Anniversary of Technical University of Szczecin, the oldest technical university of West Pomerania, as well as of many scientific technical societies of the town, namely : that of electricians, geodesists, mechanical engineers and technicians, water engineers and technicians as well as the Federation of Scientific Technical Societies NOT (Naczelna Organizacja Techniczna).

The jubilee was celebrated under the slogan :

Youth and Engineering – a chance to developing the Town and Region,

which has had a very distinct meaning.

It was arranged by the following organizations :

- the Federation of Scientific Technical Societies NOT, Szczecin
- Szczecin Division of the Polish Society of Electricians
- Technical University of Szczecin
- The Society of Graduates from Technical University of Szczecin.

Miscellanea

Second Edition (revised and enlarged) of the monograph titled :

On Fatigue Safety of Metallic Elements under Static and Dynamic Loads

written by Janusz Kolenda, Professor of Polish Naval University, Gdynia, has been recently published by Naval University Publishers (e-mail : b.szyniec@amw.gdynia.pl)

The main idea behind this monograph was to formulate energy-based design criteria accounting for the effect of static loads as well as mean and residual stresses on fatigue performance under either periodic or random loads. For this purpose the original stresses have been modelled by novel equivalent (reduced) stresses and Soderberg's equation was used.

Closed - form solutions consistent with Miles formula for the fatigue life and Parsevals formula for the power of periodic signals, have been obtained. The emphasis has been put on how to cover both the static strength conditions and fatigue safety requirements under combined static and dynamic loads.

The book (marked ISBN 83 - 87280 - 94 - 1) consists of two parts divided into two and three chapters, respectively.

Part I is devoted to the loading cases in which the stress level lies below the fatigue "safe - life" limit.
Part II is concerned with the high - cycle fatigue regime in which a finite fatigue life is expected.

Chapters 1 and **3** deal with design criteria in deterministic approach.
In **Chapters 2** and **4** probabilistic design criteria are developed.
In **Chapter 5** high - cycle fatigue criteria for anisotropic metals are considered.

Three appendices highlight the following detail problems :

A. Semiprincipal stress systems
B. On the relation between probability density functions of maximum values of original and equivalent stresses.
C. Application of the theory of energy transformation systems to fatigue assessment of metallic elements under steady loading conditions.

The book consists of 166 pages and includes 81 reference sources as well as many example calculations which greatly enrich its didactic merits.

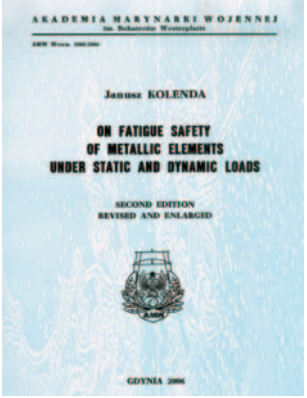

Miscellanea

RINA - KORAB Award 2006

As in the year 2005, in autumn 2006 was settled the competition for the most outstanding M.Sc. project elaborated and defended at Faculty of Ocean Engineering and Ship Technology, Gdańsk University of Technology in the academic year 2005/2006.

The competition has been arranged by :

✶ the Polish Society of Naval Architects and Marine Engineers KORAB
✶ the Royal Institution of Naval Architects - - RINA, UK
✶ Faculty of Ocean Engineering and Ship Technology, Gdańsk University of Technology.

From among 9 projects submitted to the competition the Piotr Jałowski's project on "***Stern quarter ramp/door for 6700 car capacity car carrier built in Okpo Daewoo shipyard***" won the award in question. The project was worked out under supervision of Prof. Zygmunt Paszota.

Miscellanea

75 Years of Education

In 2006 75 years went by of education of Polish Navy technical corps officers, which began with establishing Engineering Division in the then Polish Navy OfficerTrainees School in 1931. Already after a few years it bore fruits in the form of unaided building ships, and generally, maintaining high technical serviceability of naval ships.

In present, after intensive development changes the education of officers of Polish Navy technical corps is carried out by means of modern methods at Mechanical - Electrical Faculty, Polish Naval University in Gdynia. About high quality of the education goes to show a.o. the fact that only in the years 1995 – 1999 as many as 1417 technical projects and improvement proposals were submitted.

Identification of service failures of cylinder valves of ship piston combustion engines

Zbigniew Korczewski
Polish Naval University

ABSTRACT

This paper presents selected diagnostic problems of charge exchange system of ship piston combustion engines. Theoretical background of wear process of cylinder valves was highlighted in the aspect of identification and sources of known and identifiable states of unserviceability. The presented results of endoscopic examinations concern failures of cylinder valves of the engines installed on Polish Navy ships.

Keywords : technical diagnostics, ship diesel engine, valve timing

INTRODUCTION

Correct operation of self-ignition engine, which ensures expected performance and efficiency in steady and transient operational states, depends to a great extent on effectiveness of charge exchange in its cylinders. Quality of the process is demonstrated by values of coefficients of filling the cylinders with fresh charge, by which the so called filling efficiency is determined. Values of the coefficient are determined mainly by two factors :

- optimally selected distribution phases in the sense of ensuring the most favourable opening and closing angles of air inlet and exhaust gas ducts (cylinder filling and scavenging), in full range of possible engine load changes
- optimum velocity of air and exhaust gas flowing through inlet-outlet system, which ensures effective whirling the air flowing into cylinder.

To ensure optimum values of the parameters during ship engine service it is necessary to reach the full serviceability state of cylinder valves which constitute its structural parts most thermally and mechanically loaded. Specially sensitive elements are outlet valves washed by exhaust gas having the temperature above 1000 K. In such service conditions they are to fulfil additional requirements as regards heat exchange and resistance to abrasion and impact load in high temperature, as well as high demands concerning corrosion resistance.

MECHANISM OF GENERATING FAILURES OF CYLINDER VALVES

During its operation the cylinder valve is forced to move along its spindle in the guides which undergoes friction wear. The process goes at high temperature of the spindle whose additional task is to absorb heat from valve head. As a result an excessive increase of radial clearance is produced between the guide and spindle, which leads to an undesirable skew of the valve resulting in loss of cylinder tightness, gas eruption, lubricant leakage from the spindle – guide precision pair until intensive wear of the entire valve unit is reached. The phenomenon may especially intensively develop in the case of supplying the engine with fuel oil of high sulphur content. The cases are known of completely burned-out valves as a subsequent result of extensive wear of valve guide [7]. In extreme case, cracking the valve spindle, its falling down into cylinder space and subsequent failures of the „piston – piston rings – cylinder" system (TPC), including piston cracking, can happen. An observable symptom of worn valve guides are smoked valve springs, that indicates a lack of tightness of combustion chamber.

Another, often found failure of cylinder valves is a drop of elasticity of tightening springs and even their fatigue failures [4,7]. In such situation also loss of cylinder tightness can happen during its filling when the springs of outlet valves are cracked, and also during gas exhaust process when the springs of inlet valves are cracked.

THEORETICAL BACKGROUND OF WEAR PROCESS OF VALVE GUIDES AND SPINDLES

From the equilibrium condition of the forces acting on the valve at the initial instant of its opening (Fig.1) it results that the force, R, generated by distribution shaft cam pressure acting onto the valve spindle face, is balanced by the sum of the cylinder gas pressure force, P_g, acting onto valve head, the valve mechanism inertia force P_b and the spring tension force P_s, according to the equation :

$$R = P_g + P_b + P_s \quad (1)$$

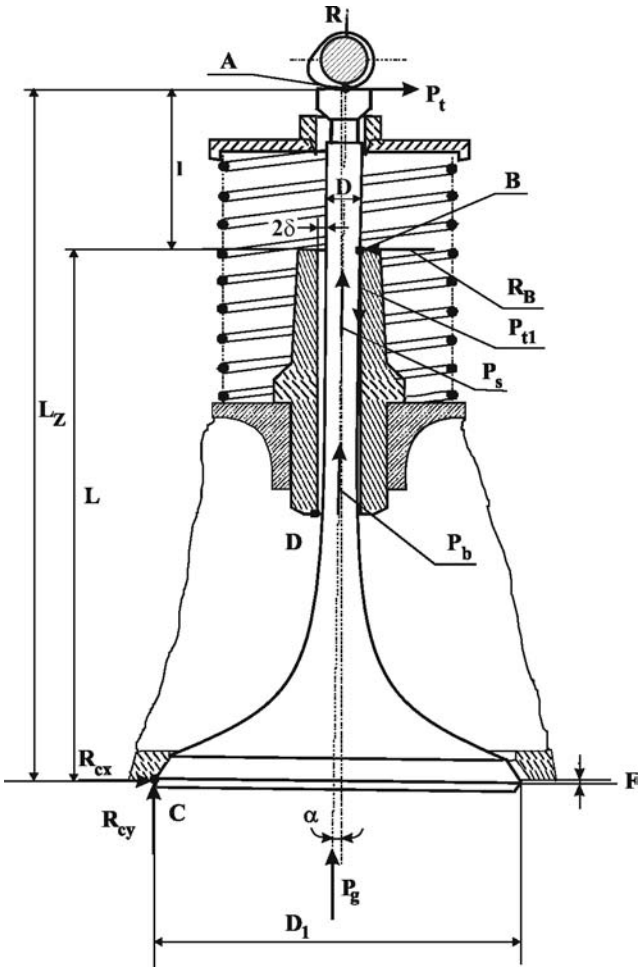

Fig. 1. *Schematic diagram of the forces acting onto cylinder valve at the initial instant of its opening .*

Due to cam sliding over valve spindle face the additional friction force P_t resulting in side pressure forces of the spindle moving inside the guide, is produced :

$$P_t = R\mu \tag{2}$$

where : μ – sliding friction coefficient in the point A.

In the same time due to action of the force R in the point B, apart from the lateral force R_B, appears the friction force P_{t1} which becomes the direct cause of valve guide wearing :

$$P_{t1} = R_{B1}\mu_1 \tag{3}$$

where : μ_1 – sliding friction coefficient in the point B.

Values of the coefficients μ and μ_1 depend on material properties of sliding elements, as well as on a degree of smoothness and dryness of contact surface. However, they do not depend on a size of contact surface (unless its area is so small that pressure force can deform it).

As in the spindle-guide precision pair always certain radial clearance δ dependent on the spindle diameter D appears, during valve opening certain deviation, α, of coaxiality of valve guide and spindle is generated. However in the case of an excessive wear of the guide and increased radial clearance at the instant when cam pressures on the valve spindle, before the valve head becomes separated from valve seat, the gap F appears on one side of the seat face, that leads to loss of valve tightness, but on its other side the valve head is pressed onto the valve seat in the point C, that leads to valve spindle bending in the direction of action of the force P_t (around the point C). Consequently through the developed gap hot cylinder gases get out with high velocity, which results in local overheating the valve head and seat materials, as well as in forming local erosion pits in valve seat face, Fig.2.

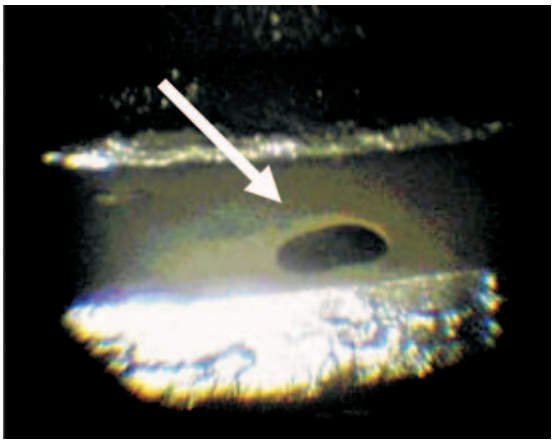

Fig. 2. *M401A-1 engine − the outlet valve head of the cylinder no. 1 − traces of erosion wear of valve seat face .*

Analysing the distribution of the forces acting onto the valve, shown in Fig.1 one can observed that due to action of the friction force P_t in the points B and C of the valve spindle - guide contact as well as the contact in the valve seat face, the reaction forces R_B and R_{Cx}, respectively, appear which generate the bending moments M_B and M_C in those points. It should be also observed that the force system is dynamic, i.e. that in which load is changing continually. In quasi-stationary approach the force resultants can be determined by using the condition of equilibrium of forces and moments, as follows :

$$\sum P_{ix} = 0 \Rightarrow R_{Cx} - R_B + P_t = 0 \tag{4}$$

hence :

$$R_{Cx} = R_B - P_t \tag{5}$$

$$\sum P_{iy} = 0 \Rightarrow R_{Cy} + P_g + P_b + P_s - P_{t1} - R = 0 \tag{6}$$

Assuming that at a given instant the sum of the forces acting onto the system is constant one obtains the following :

$$P_w = P_g + P_b + P_s - R \tag{7}$$

Then the sum of bending moments respective to the point C is as follows :

$$\sum M_{iC} = 0 \Rightarrow P_w\left(\frac{D_1}{2} + \delta\right) + \\ - P_{t1}\left(\frac{D_1}{2} + \frac{D}{2} + \delta\right) + R_B L - P_t L_Z = 0 \tag{8}$$

hence :

$$P_w\left(\frac{D_1}{2} + \delta\right) - R_B\left[\mu_1\left(\frac{D_1 + D + 2\delta}{2}\right) - L\right] - R\mu L_Z = 0 \tag{9}$$

The reaction force in the point B, which decides on the rate of wear of the upper part of the valve guide, is then the following :

$$R_B = \frac{P_w(D_1 + 2\delta) - 2R L_z \mu}{\mu_1(D_1 + D + 2\delta + 2L)} \tag{10}$$

Making use of the relation (7) one finally obtains the following :

$$R_B = \frac{(P_g + P_b + P_s)(D_1 + 2\delta) - R(D_1 + 2\delta + 2L_z\mu)}{\mu_1(D_1 + D + 2\delta + 2L)} \tag{11}$$

When the relation (3) is taken into consideration one can determine the value of friction force in the upper part of the valve guide :

$$P_{t1}=\frac{(P_g+P_b+P_s)(D_1+2\delta)-R(D_1+2\delta+2L_z\mu)}{D_1+D+2\delta+2L} \quad (12)$$

Making use of the relation (5) one can also determine the reaction force in the point C, which decides on the rate of wear of the valve seat face :

$$R_{Cx}=R_B-R\mu \quad (13)$$

Considering the system of the forces acting onto the valve at the instant of separation of the valve head from the valve seat, Fig.3, one can observe that the spindle presses the lower part of the valve guide in the point D (the support point C disappears).

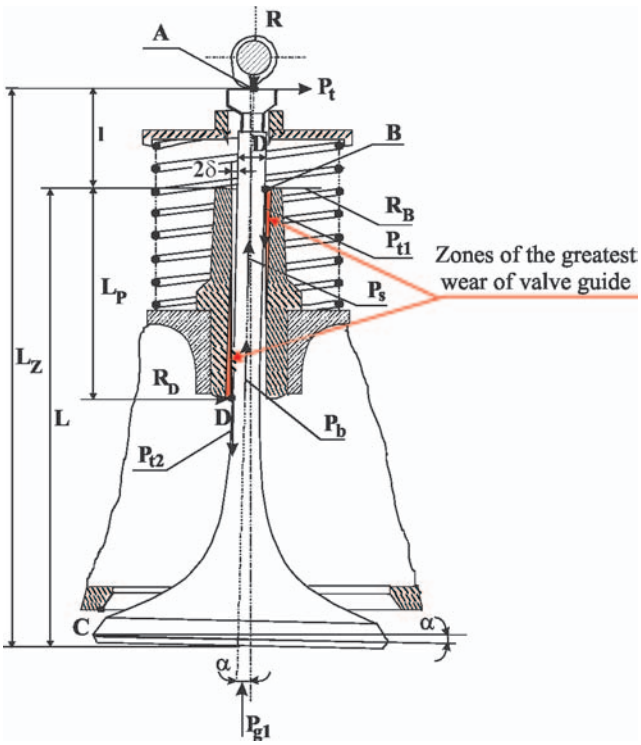

Fig. 3. *Schematic diagram of the forces acting onto the cylinder valve at the instant of its full separation from the valve seat .*

Under influence of the force R in the points B and D, apart from the transverse forces R_B and R_D, the respective friction forces P_{t1}, P_{t2} are induced, which become the direct cause of the valve guide wearing in its upper and lower part :

$$P_{t1}=R_B\mu_1 \quad (14)$$

$$P_{t2}=R_D\mu_1 \quad (15)$$

where :

μ_1 – sliding friction coefficient in the points B and D.

In such situation the reaction forces R_B and R_D, resulting from the friction force P_t, generate the respective bending moments M_B and M_D in the points B and D. Making use of the conditions of equilibrium of forces and moments one obtains the following :

$$\sum P_{ix}=0 \Rightarrow R_D-R_B+P_t=0 \quad (16)$$

hence :

$$R_D=R_B-R\mu \quad (17)$$

$$\sum P_{iy}=0 \Rightarrow -P_{t1}+P_{g1}+P_b+P_s-P_{t2}-R=0 \quad (18)$$

By assuming that at the given instant the sum of the forces acting onto the system is constant the following is obtained :

$$P_{w1}=P_{g1}+P_b+P_s-R \quad (19)$$

On insertion of (19) to the relation (18) the following is yielded :

$$P_{w1}-P_{t1}-P_{t2}=0 \quad (20)$$

When the relations (14), (15) and (17) are taken into account the reaction force in the point B, which decides on the rate of wear of the upper part of the valve guide :

$$R_B=\frac{P_{w1}+R\mu_1\mu}{2\mu_1} \quad (21)$$

as well as the reaction force in the point D, which determines the rate of wear of the lower part of the valve guide, can be determined :

$$R_D=\frac{P_{w1}-R\mu_1\mu}{2\mu_1} \quad (22)$$

In Fig. 3 the zones of the greatest rate of wear of the valve guide are marked red.

Summing up the above performed considerations one can enumerate the design factors determining the reaction forces R_C, R_B and R_D, which detrimentally influence the design structure of valve spindle guides :

- the height of spindle above valve guide, l, which should be as small as possible
- the valve guide length L_p as well as the distance from the upper edge of the guide to the seat face of valve head, L, which should be as big as possible
- value of the friction force P_t generating side pressure forces of the spindle moving along the guide, which should be kept as small as possible.

The last design factor decreasing wear of cylinder valves is controlled by changing the character of valve rocker friction against the valve spindle face – from sliding friction to rolling one. As shown in Fig.4 it is possible by mounting the rollers at the rocker's end cooperating with the valve spindle.

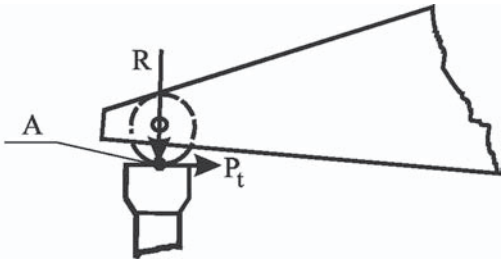

Fig. 4. *Schematic diagram of the forces acting in the " valve rocker with roller – face of valve spindle" system .*

Introducing simplifications, one can assume that the roller which substitutes the cam, generates only the pressure force R applied to the valve, in absence of any friction force P_t (its value is about ten times smaller than that in the case of sliding friction) [5]. Then no side components responsible for wearing the guide will be produced. The system will be in the state of equilibrium described by the relation (1). However because of the drop of elasticity (relaxation) of the valve spring, its service wear, wear of spindle face and valve head, certain transverse reaction leading to guide wearing will be always produced and the system will reach the equilibrium shown in Fig.1, except that in the point A no friction force P_t will be present.

From the condition of equilibrium of forces and moments the reaction forces are determined as follows :

$$R_{Cx} = R_B \tag{23}$$

$$R_{Cy} + P_g + P_b + P_s - P_{t1} - R = 0 \tag{24}$$

The friction force in the point B, which determines valve guide wearing, is described as follows :

$$P_{t1} = R_B \mu_1 \tag{25}$$

where : μ_1 – sliding friction coefficient in the point B.

Assuming as before that at a given instant the sum of forces acting onto the system is constant (7) one obtains the expression which describes the sum of bending moments respective to the point C :

$$\sum M_{iC} = 0 \Rightarrow P_w\left(\frac{D_1}{2} + \delta\right) + - P_{t1}\left(\frac{D_1 + D + 2\delta}{2}\right) + R_B L = 0 \tag{26}$$

hence :

$$P_w\left(\frac{D_1}{2} + \delta\right) - R_B\left[\mu_1\left(\frac{D_1 + D + 2\delta}{2}\right) - L\right] = 0 \tag{27}$$

Hence the reaction force in the point B, which decides on the rate of wear of the upper part of valve guide, is as follows :

$$R_B = \frac{P_w(D_1 + 2\delta)}{\mu_1(D_1 + D + 2\delta) - 2L} = R_{Cx} \tag{28}$$

It is quantitatively equal to the reaction force in the point C, which decides upon the rate of wear of valve seat face.

The expression which describes the sum of bending moments respective to the point B, obtains the following form :

$$\sum M_{iB} = 0 \Rightarrow -R_{Cy}\left(\frac{D_1 + D + 2\delta}{2}\right) + + R_{Cx} L - P_w\left(\frac{D + 2\delta}{2}\right) = 0 \tag{29}$$

Hence the vertical component of the reaction force in the point C is expressed by the following formula :

$$R_{Cy} = \frac{2R_{Cx}L - P_w(D + 2\delta)}{D_1 + D + 2\delta} \tag{30}$$

Applying the analogical considerations to the system shown in Fig. 3 where the roller is used instead the cam to neglect the friction force P_t in the point A, one can determine the equilibrium equations for the following forces :

$$\sum P_{ix} = 0 \Rightarrow R_D = R_B \tag{31}$$

$$\sum P_{iy} = 0 \Rightarrow -P_{t1} + P_{g1} + P_b + P_s - P_{t2} - R = 0 \tag{32}$$

Assuming that at a given instant the sum of forces acting onto the system is constant one obtains the following :

$$P_{w1} = P_{g1} + P_b + P_s - R \tag{33}$$

Inserting it into (32) one obtains :

$$P_{w1} - P_{t1} - P_{t2} = 0 \tag{34}$$

After taking into account the conditions :

$$P_{t1} = \mu_1 R_B \quad \text{and} \quad P_{t2} = \mu_1 R_D \Rightarrow P_{t1} = P_{t2} \tag{35}$$

one can determine the reaction forces in the points B and D, which decide upon the rate of wear of the upper and lower part of valve guide :

$$R_B = \frac{P_{t1}}{\mu_1} = \frac{P_{t2}}{\mu_1} = \frac{P_{w1}}{2\mu_1} = \frac{P_{g1} + P_b + P_s - R}{2\mu_1} = R_D \tag{36}$$

From comparison of the expressions (21), (22) and (36) which describe the reaction forces in the support points B and D, for the system fitted with the distribution shaft cam and that with the valve arm roller, respectively, it results that the use of the roller makes the rates of wear of upper and lower part of valve guide equal. And, the greater the radius of the roller the smaller the rate of wear. At the initial instant of valve opening the rate of wear of valve seat face will be also lower due to a significant decrease of the reaction force in the point C.

EXAMINATIONS OF CYLINDER VALVES OF SHIP DIESEL ENGINES DURING SERVICE

Novel methods of diagnostic tests are commonly introduced into operation process of ship diesel engines. The dynamically developing endoscopy which has been earlier applied only in medical examinations, now serves as a very useful, even indispensable tool for assessing the technical state of complex ship engines.

Endoscopy is a disassembling-free method for visual - optical inspection of interior of machines and devices by means of specular instruments (endoscopes).

For endoscopic examinations of the engines installed on Polish Navy ships the following instruments are used : IF8D4−15 fiberscope and a kit of borescopes of OLYMPUS and STORZ firms, differing to each other by the length of optical system, its diameter and angle of observation of a diagnosed element, namely : 90cm/8mm/90°, 55cm/8mm/90°, 45cm/8mm/90°, 50cm/6mm/90°, 30cm/4mm/0°, 30cm/10mm/120° – see Fig.5. The instruments make it possible to examine and prepare photographic documentation of engine's internal elements, through inspection openings having their diameter greater than 5 mm. A special digital photo-camera, Camedia C−2500L made by OLYMPUS firm, is used to perform dimensional analysis of detected failures, visualize them and record in a data base.

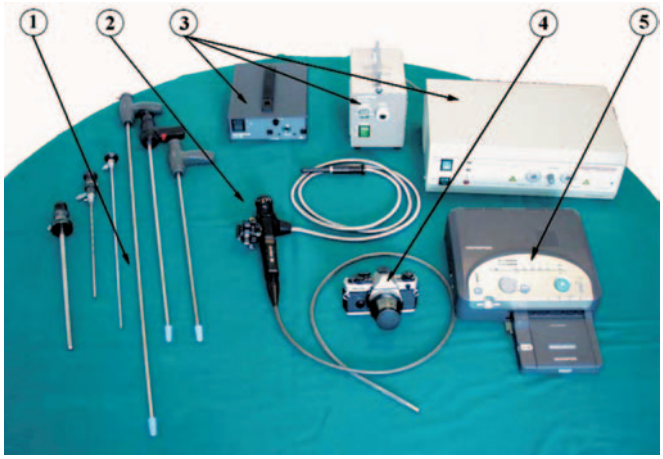

Fig. 5. *The endoscopic diagnostic system of OLYMPUS firm : **1** − kit of borescopes, **2** − fiberscope, **3** − kit of light sources, **4** − digital photo-camera, **5** − photo-printer .*

The camera is connected with a borescope or fiberscope by means of special links (adapters).

The length of the fiberscope's elastic light pipe whose controllable end makes observation in an arbitrary direction possible, is equal to 1500 mm. It has replaceable ends making observation within front and side sectors of different observation angles possible. Owing to this, to a great extent are increased manual possibilities of inspection of interior of air and exhaust gas flow passages of engine and turbo-compressor system.

Borescopes of different lengths and rigid optical system make it possible to carry out observations within front and side sectors in a wide range of variability of observation angle. The 30cm/10mm/120^{0}optical system is especially useful in diagnosing the engine combustion chambers, the valve seats fixed in lower plate of engine head in particular. Borescopes are also very useful during inspection of guide vanes and moving blades of turbo-blower.

In Fig.6 is presented a way of conducting the endoscopic examinations of ship engine cylinder systems by using a borescope and fiberscope. And, in Fig. 6 is presented a way of getting access to interior of the cylinder liner of the ship diesel engines : M401A-1(2) and 16V149TI Detroit Diesel, for endoscopic examinations.

a)

b)

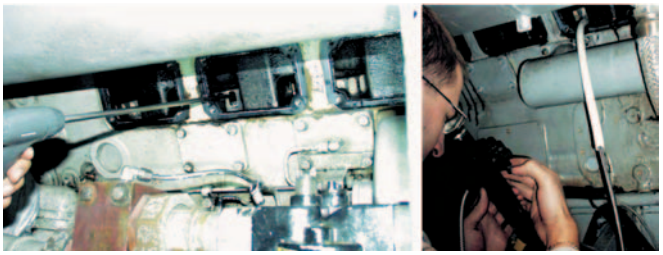

Fig. 6. *Ways of inserting the end of borescope and fiberscope into cylinder interior of :* ***a)*** *M401A-1 diesel engine – through the holes remaining from dismounted injectors,* ***b)*** *16V149TI Detroit Diesel engine – through inlet air windows in cylinder liner .*

When the injector is dismounted the borescope (fiberscope) makes it possible to assess technical state of piston head, cylinder liner surface, cylinder head and other units fixed in it such as spray nozzles of remaining injectors, inlet and outlet valves, starting valves etc (Fig.7). The endoscopic method of inspection is especially useful in diagnosing multi-block and multi-cylinder engines. For instance, in the case of radial engines, e.g. the M503 or M520 engine already installed in the engine room, an access to its lower mono-blocks and lower parts of reduction – reversing gear is very difficult. In order to perform inspection of the engines together with their gears they must be uncoupled from propeller shaft, next inclined and lifted and sometimes even rotated inside the engine room so as to make the first or seventh cylinder block accessible. From operational practice it results that a fiberscope of a sufficiently long light pipe makes it possible to avoid those inconveniences and thus to save execution time of overhauls and associated costs even by 25-30% [7].

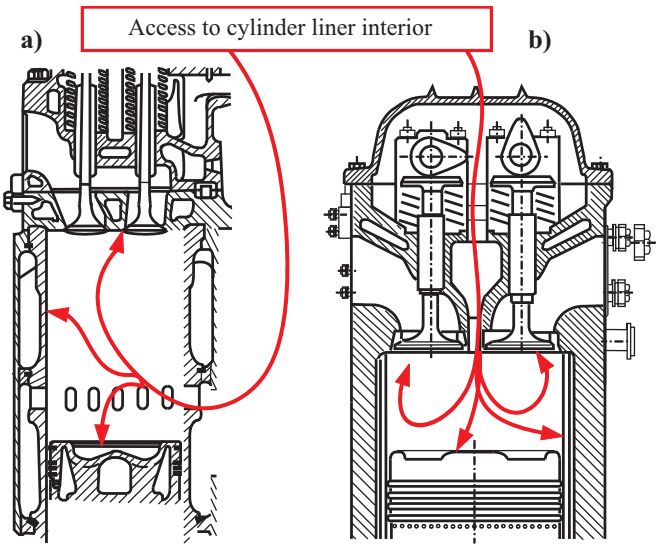

Fig. 7. *Endoscopic examination of ship engines – access to cylinder liner interior:* ***a)*** *16V149TI Detroit Diesel engine,* ***b)*** *M401A-1(2) diesel engine .*

FAILURES OF CYLINDER VALVES OF SHIP ENGINES

Systematic endoscopic examinations of ship engines installed on Polish Navy ships are carried out in the following situations :

- during preventive surveys (once a year at least)
- at current assessment of technical state of an engine when to prolong the time between repairs is necessary
- in the case of an increased vibration level, found metal particles in lubricating oil, occurrence of sudden deviations from the trend line of mean indicated pressure (indicated power) in a cylinder, increased exhaust gas temperature, excessive smoke emission etc.
- when to dismount the engine head is difficult and time-consuming.

On the basis of multi-year endoscopic examinations of ship engines a procedure of their technical state assessment in service conditions was elaborated. It contains the necessary scope and scheduling principles of examinations of engine interior, aimed at detection of possible defects of particular elements of functional systems of the engine. For every type of the engines used on Polish Navy ships detail instructions for realization of diagnostic examinations by means of the fiberscope and kit of borescopes, were elaborated. The identified failures are photographically recorded to make documentation of the detected defects and to determine a tendency of their development. Results of the examinations are saved in a computer data base [1,2,3,7].

High effectiveness of the method in question, at a relatively simple use of the diagnosing instruments, has been confirmed during almost 15 years of experience in endoscopic examining the ship engines, gained by specialists from Polish Naval University. As a result of the performed examinations were identified many material defects which could be transformed into serious hazards to engine reliability in the case of their further development.

The selected failures of cylinder valves of ship diesel engines, identified during endoscopic inspections in service, are presented in Fig.8 and 9 [1,2,3 and 7].

The heavy oiling-up of inlet and outlet valves goes to show that the valve spindle guides are excessively worn. In order not to allow for premature wearing-out the guides and for bending the valve spindles, that always leads to loss of tightness of

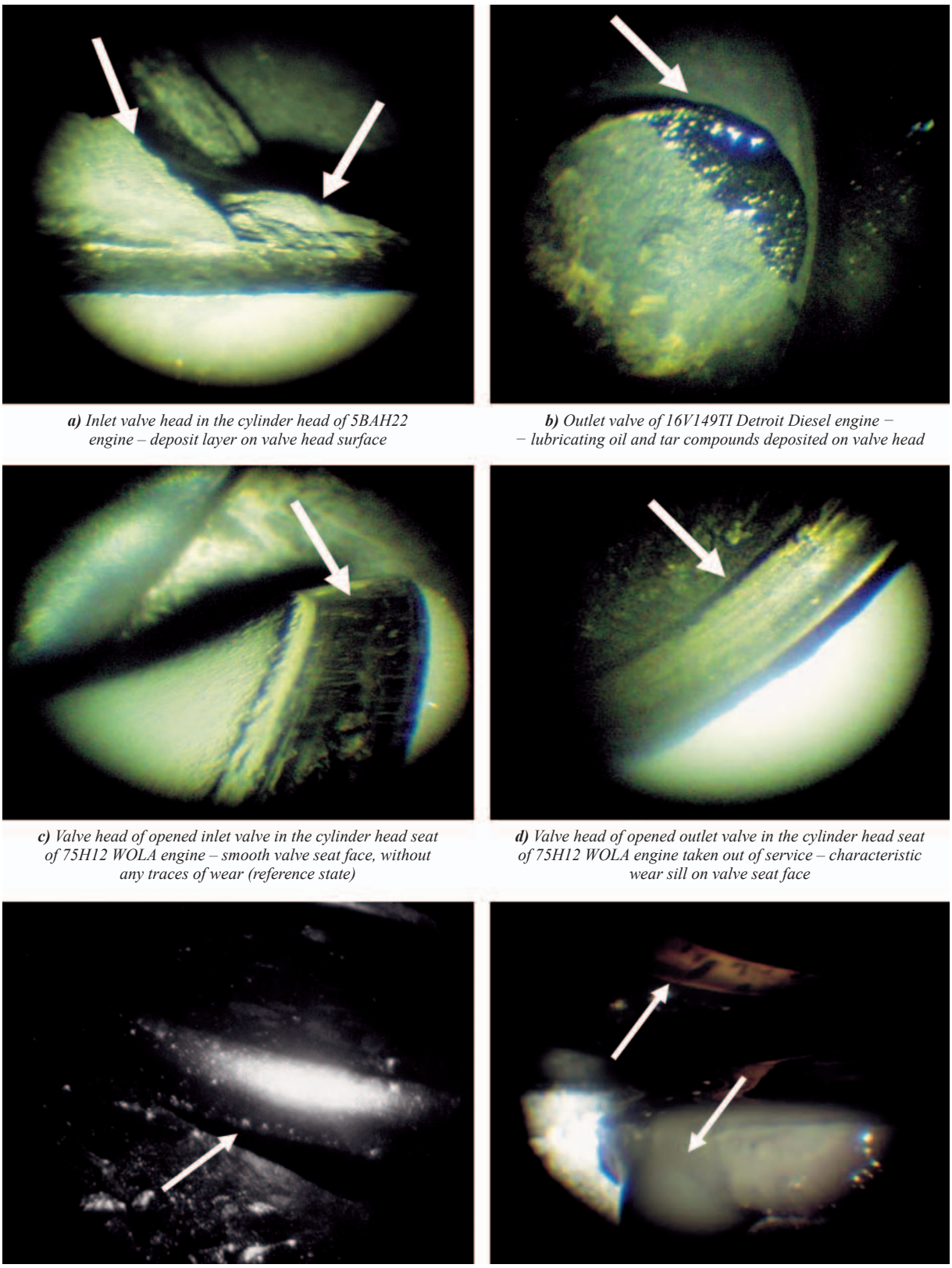

a) *Inlet valve head in the cylinder head of 5BAH22 engine – deposit layer on valve head surface*

b) *Outlet valve of 16V149TI Detroit Diesel engine – – lubricating oil and tar compounds deposited on valve head*

c) *Valve head of opened inlet valve in the cylinder head seat of 75H12 WOLA engine – smooth valve seat face, without any traces of wear (reference state)*

d) *Valve head of opened outlet valve in the cylinder head seat of 75H12 WOLA engine taken out of service – characteristic wear sill on valve seat face*

e) *Outlet valve of M503A engine – loss of valve tightness due to bent valve spindle*

f) *Inlet valve head in the face of cylinder head of M401A-2 engine – oil layer (visible oil drop) on valve head surface, smooth valve seat face, without any traces of wear and corrosion*

Fig. 8. *Defects of ship diesel engines, identified during endoscopic examinations .*

cylinders, two values of radial clearance between the guide and spindle are provided :

- ☆ optimum one, i.e. that for assembling
- ☆ ultimate one, i.e. that qualifying a given valve for replacement or regeneration.

It is recommended to keep the assembling values of radial clearance of inlet valves, related to the valve spindle diameter D, within the range of (0.004 ÷ 0.006) D and their ultimate values – within the range of (0.01 ÷ 0.015) D, which means that the radial clearance value may increase even 2 ÷ 3 times during engine service. In the case of outlet valves the respective

values of radial clearance amount to : (0.006 ÷ 0.01)D – for assembling, and (0.015 ÷ 0.025) D – ultimate ones [6].

The ultimate value of radial clearance results from the permissible bend (curvature) of valve spindle moving within valve guide. A measure of the bend can be the angle α which determines coaxiality of the spindle and guide, or the gap F which appears on the valve seat face. (Fig. 1 and 3). As results from the system of forces acting onto cylinder valve, shown in

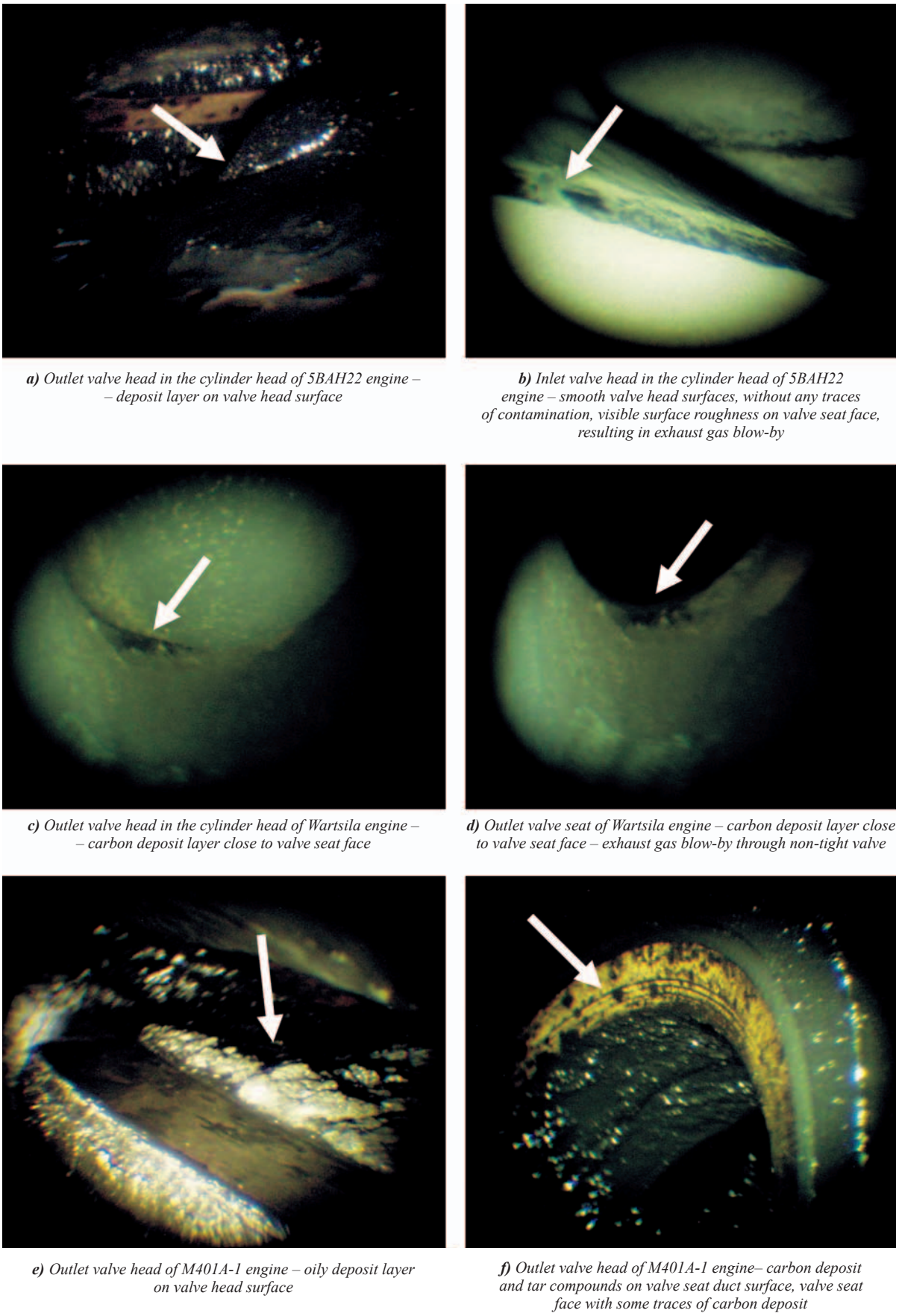

a) *Outlet valve head in the cylinder head of 5BAH22 engine – – deposit layer on valve head surface*

b) *Inlet valve head in the cylinder head of 5BAH22 engine – smooth valve head surfaces, without any traces of contamination, visible surface roughness on valve seat face, resulting in exhaust gas blow-by*

c) *Outlet valve head in the cylinder head of Wartsila engine – – carbon deposit layer close to valve seat face*

d) *Outlet valve seat of Wartsila engine – carbon deposit layer close to valve seat face – exhaust gas blow-by through non-tight valve*

e) *Outlet valve head of M401A-1 engine – oily deposit layer on valve head surface*

f) *Outlet valve head of M401A-1 engine– carbon deposit and tar compounds on valve seat duct surface, valve seat face with some traces of carbon deposit*

Fig. 9. *Defects of ship diesel engines, identified during endoscopic examinations .*

Fig. 3, the angle of valve spindle bend is equal to the angle of skew of valve head in compliance with the expression:

$$\alpha = \frac{2\delta}{L_P} = \frac{F}{D_1} \tag{37}$$

The quantities are determined, at the same values of radial clearance, by the following design parameters :

- ⇨ guide length
- ⇨ valve spindle length
- ⇨ valve head diameter
- ⇨ mutual location of the spindle and guide

From the expression (37) it results that the dimensions of the gap of valve seat face, F, increase when the radial clearance between guide and spindle, δ, increases, the greater the valve head diameter D_1, and the smaller the guide length L_p :

$$F = \frac{2\delta D_1}{L_P} \tag{38}$$

From the relation (38) it also results that in the case of the predetermined permissible value of the valve seat face gap, F, the greater the guide length L_p and the smaller the valve head diameter D_1, the greater the ultimate value of the radial clearance δ :

$$\delta_{gr} = \frac{FL_P}{2D_1} \tag{39}$$

Additionally, worth mentioning that the ultimate value of the radial clearance does not depend on the valve spindle diameter D.

For the considered ship diesel engines the radial clearance values of inlet and outlet valves are presented in Table [6].

Table. *Assembling and ultimate values of the radial clearance between the spindle and guide of inlet and outlet valves of the engines : M401A-1(2) and 16V149TI Detroit Diesel .*

Type of engine	Inlet valves			Outlet valves		
	Valve spindle diameter [mm]	Assembling clearance value [mm]	Ultimate clearance value [mm]	Valve spindle diameter [mm]	Assembling clearance value [mm]	Ultimate clearance value [mm]
M401A-1(2)	18.00	0.094	0.144	17.93	0.099	0.149
16V149TI Detroit Diesel	Gap-valve distribution system			9.44	0.026	0.055

CONCLUSIONS

- Leakage of lubricating oil from valve guide is a symptom of dropping compression pressure in engine cylinder as a result of loss of tightness of combustion chamber.
- Rate of wear of cylinder valve guide depends on pressure force exerted by valve spindle onto valve guide wall, and on their mutual sliding.
- And, velocity of the sliding is directly proportional to the mean piston velocity and crankshaft rotational speed.

NOMENCLATURE

D – diameter of valve spindle
D_1 – diameter of valve head
F – height of valve face gap
l, L – height, length
M – moment of force
P, R – force
p – pressure

α – angle
δ – radial clearance between valve spindle and guide
μ – sliding friction coefficient in the point A
μ_1 – sliding friction coefficient in the points B_1 and D
τ – time

Indices and abbreviations

b – of inertia
g – of gases
gr – an ultimate quantity
p – of guide
s – of spring tension
t – of friction
w – a resultant quantity
x,y – a component quantity
z – of valve
A, B, C, D – points of contact (support) of valve system elements
TPC – the„ piston – piston rings- cylinder" system
ZS – self ignition

BIBLIOGRAPHY

1. Korczewski Z.: *Endoscopic examination of naval gas turbines*. Polish Maritime Research, No. 4/1998
2. Korczewski Z., Pojawa B.: *Endoscopic diagnostics of ship engines* (in Polish). 32nd Domestic Symposium „Diagnostics of Machines". Węgierska Górka, 28.02-05.03.2005
3. Korczewski Z., Pojawa B.: *Diagnosing ship combustion engines by means of endoscopes* (in Polish). 7th Scientific Technical Symposium „Combustion engines in military applications"- „SILWOJ'2005". Rynia, 26-28.10.2005
4. Piaseczny L.: *Repair technology of combustion engines* (in Polish). Maritime Publishing House (Wydawnictwo Morskie), Gdańsk, 1992
5. Wajand J. A., Wajand J. T.: *Medium and high speed piston combustion engines* (in Polish). Scientific Technical Publishing House (WNT). Warszawa, 2005
6. Detroit Diesel : *Technical and operational documentation of M401A-1(2), M503 and M520 gas turbines*
7. *Reports on diagnostic examinations of piston combustion engines installed on Polish Navy ships* (in Polish). Research reports of Polish Navy University (Prace badawcze AMW), Gdynia, 1992 ÷ 2005

CONTACT WITH THE AUTHOR
Assoc. Prof. Zbigniew Korczewski
Mechanic-Electric Faculty,
Polish Naval University
Śmidowicza 69
81-103 Gdynia POLAND
e-mail: zkorczewski@wp.pl

Calculation of the mean long-term service speed of transport ship

Continuation of the second part of the paper published in the Polish Maritime Research No.1(51), January 2007

Part III
Influence of shipping route and ship parameters on its service speed

Tadeusz Szelangiewicz
Katarzyna Żelazny
Szczecin University of Technology

ABSTRACT

Service speed obtainable by a ship in real weather conditions when sailing on a given shipping route, is one of the major parameters which have great impact on ship operation costs. The so far used, very approximate method of service speed prediction based on "service margin", is very little exact. In this paper a new method based on additional ship resistance dependent on mean statistical parameters of wave and wind occurring on a given shipping route, is presented. The mean long-term service speed is calculated on the basis of the calculated additional resistance and the screw propeller and propulsion engine parameters. Also, a new definition of service margin and a way of its calculation is presented apart from the results of the mean service speed calculation depending on ship's type and size and shipping route.

Keywords : ship service speed, wind, waving, shipping route, service margin, long-term prediction.

PARAMETERS OF THE SHIPS FOR WHICH CALCULATIONS WERE PERFORMED

Calculations of the mean additional resistance and mean long-term service speed were performed for 7 existing ships of determined propulsion systems and 15% service margin. They represented two types of ships : bulk carriers and containerships of different size. The main parameters of the ships are given in Tab.4.

All calculations for each ship were performed for constant ship's draught and constant state of hull and propeller surface, that made it possible to more accurately compare the ships sailing on a given shipping route, by taking into account ship's type and size. The used computer software has been so designed as to make it possible to perform calculations at variable draught (considered as a random variable of a given occurrence probability) and for changeable state of hull and propeller surface.

SHIPPING ROUTES

For the calculations of the mean additional resistance and mean long-term service speed the most representative shipping routes were selected on the basis of [1]. They are specified in Tab.5 and shown in Fig.16.

All additional data which describe ship's voyage on a given shipping route (i. e. specification of sea areas crossed by the route, probability of ship's staying in a given sea area, f_A, ship's course angle ψ and probabilities of ship's courses in a given sea area, f_ψ) can be found in [4].

Tab. 4. *Ship main parameters .*

Ship / Data	Symbols	Container--ship K1	Container--ship K2	Container--ship K3	Bulk carrier M1	Bulk carrier M2	Bulk carrier M3	Bulk carrier M4
Length b.p.	L [m]	140.14	171.94	210.20	138.0	185.0	175.6	240.0
Breadth	B [m]	22.30	25.30	32.24	23.0	25.3	32.2	32.2
Draught	T [m]	8.25	9.85	10.50	8.55	10.65	12.05	11.6
Displacement at T	∇ [m^3]	17300	29900	47250	21441	40831	56396	73910

Contract speed	V_K [m/s]	8.44	9.62	10.80	7.15	7.72	8.2	8.28
Propeller diameter	D_p [m]	5.2	6.15	7.42	5.0	5.8	6.2	6.5
Propeller pitch	P [m]	3.9	5.8	6.8	4.2	3.9	5.7	4.5
Engine rated power	N_n [kW]	6930	13750	26270	4710	7500	12000	12720
Driving engine rated speed	n_n [1/s]	2.33	1.82	1.72	1.85	2.03	1.64	1.93
Still - water resistance of ship for T and V_K	R [kN]	461.3	858.8	1477.5	405.9	600.4	865.6	947.6
Service margin assumed in propulsion system design	$k_ż$ [%]	15	15	15	15	15	15	15

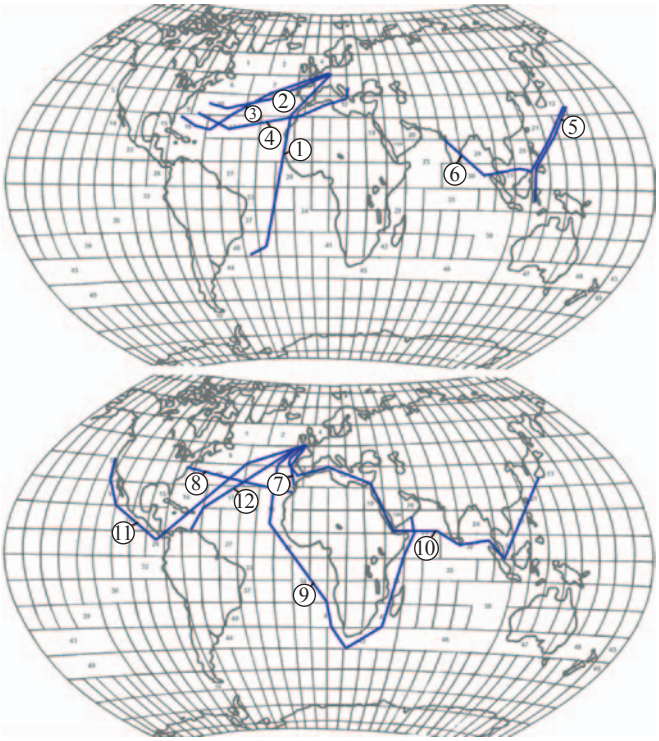

Fig. 16. *Runs of the shipping routes for which calculations were performed .*

In each case the calculations were performed for both legs of voyage (there and back) hence every shipping route has two indices : **a** and **b** (e.g. shipping route no. 2 → 2a and 2b).

Tab. 5. *Specification of the shipping routes used for calculation of additional resistance and service speed of ship .*

No.	Name
1	South America – West Europe
2	US East coast – West Europe
3	US East coast – Gulf of Mexico – West Europe
4	US East coast – Mediterranean – West Europe
5	Indonesia – Japan
6	Persian Gulf – Japan
7	North Africa – West Europe
8	North Africa – US East coast
9	Persian Gulf – Africa – West Europe
10	West Europe – Mediterranean – Persian Gulf – Japan
11	West Europe – Panama Canal – US West coast
12	West Europe – South and Central America

CALCULATION RESULTS

The calculation results for every ship and shipping route are presented in the form of bar charts for the additional resistance ΔR and service speed V_E. The speed the ship is able to achieve, was calculated under the assumption that its set value has to be maintained or its maximum value achievable in a given weather conditions at simultaneous keeping the set ship course, has to be determined. The obtained bar charts were also approximated by using the distribution functions : that of the additional resistance $f(\Delta R)$, and that of service speed $f(V_E)$, with the determined R^2 (share of the "resolved" variance), [2].

Under the bar charts for a given ship and shipping route the following data are tabularized :

- the maximum value of additional resistance, ΔR_{max}, which occurred for a given ship on a given shipping route
- the mean value of additional resistance, $\overline{\Delta R}$, calculated from the formula :

$$\overline{\Delta R} = \frac{\sum_{i=1}^{n_R} P_{TR_i} \cdot (\Delta R_i = const)}{\sum_{i=1}^{n_R} P_{TR_i}} \tag{45}$$

- the relative resistance increase, PR, calculated from the formula :

$$PR = \frac{\overline{\Delta R}}{R} \cdot 100\% \tag{46}$$

- the set value of ship service speed, V_{ZE}
- the minimum value of ship speed, V_{min}, which occurred on a given shipping route at keeping a set course
- the mean long-term value of ship speed, $\overline{V}_E$, on a given shipping route, calculated from the formula :

$$\overline{V}_E = \frac{\sum_{i=1}^{n_V} P_{TV_i} V_i (\Delta R_i = const)}{\sum_{i=1}^{n_V} P_{TV_i}} \tag{47}$$

- the probability, P_{V_E}, of maintaining the service speed, V_{ZE}, on a given shipping route at keeping a set course
- percentage of the events in which ship speed has been reduced for the reason of exceeded ship's sea-keeping criteria
- percentage of the events in which no result of calculations, i.e. no value of ship speed, has been found. The lack of solu-

tion resulted from the fact that it was assumed to keep a set course, that was not possible in very high and oblique waves - the ship course should be changed in such situations.

The calculated bar charts for all the ships (Tab.4) and all the shipping routes (Tab.5) together with the remaining results can be found in [4]. The example bar charts for **K1** ship (Tab.4) sailing there and back on the chosen route (South America – – West Europe), are presented in Fig.17.

In Fig.19 are showed the values of additional resistance index for the same ship, defined by means of the formula (46) depending on a shipping route. The index should not be identified,as for its value, with the service margin because it constitutes a definite long-term statistical quantity tightly connected with parameters of weather conditions occurring on a given shipping route, hence value of the index is changeable whereas value of the service margin assumed in design process is of a constant value. However, value of the index may suggest

Ship : K1

Shipping route no. 1a

Histogram and distribution function of additional resistance

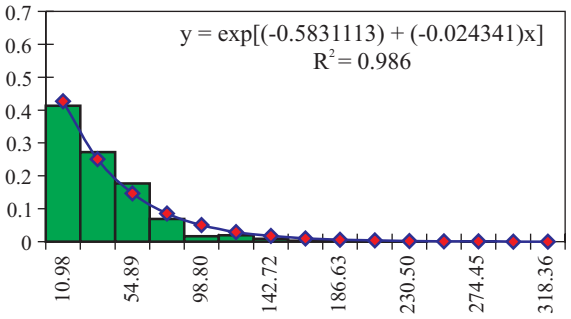

Still-water resistance at the speed V_K [kN]	R	461.26
Max. additional resistance [kN]	ΔR_{max}	367.70
Mean additional resistance [kN]	$\Delta\overline{R}$	35.77
Resistance increase [%]		7.8
Percentage of no-solution events [%]		0.11

Histogram and distribution function of service speed

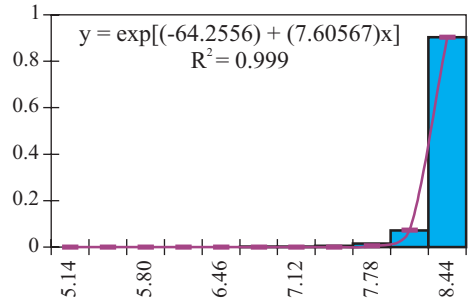

Set service speed [m/s]	V_{ZE}	8.44
Minimum speed [m/s]	V_{min}	1.88
Mean speed [m/s]	$\overline{V}_E$	8.38
Probability of V_{ZE}	P_{V_E}	0.90
Percentage of speed-reduction events [%]		0.11

Shipping route no. 1b

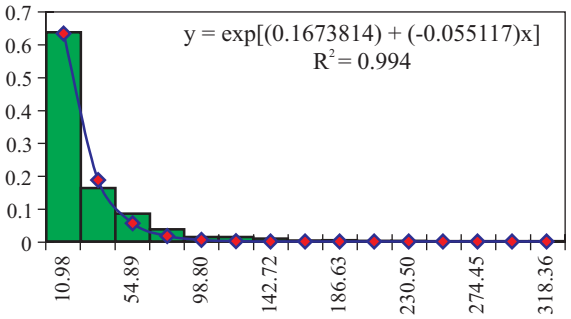

Still-water resistance at the speed V_K [kN]	R	461.26
Max. additional resistance [kN]	ΔR_{max}	365.74
Mean additional resistance [kN]	$\Delta\overline{R}$	28.02
Resistance increase [%]		6.1
Percentage of no-solution events [%]		0.22

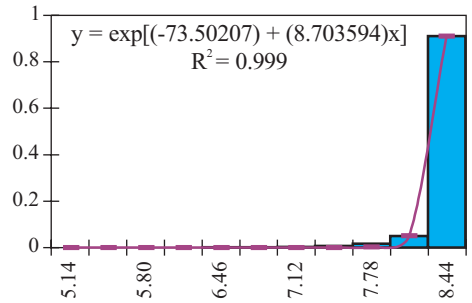

Set service speed [m/s]	V_{ZE}	8.44
Minimum speed [m/s]	V_{min}	1.88
Mean speed [m/s]	$\overline{V}_E$	8.37
Probability of V_{ZE}	P_{V_E}	0.92
Percentage of speed-reduction events [%]		0.07

Fig. 17. *Bar charts and distribution functions of additional resistance and service speed for* ***K1*** *ship .*

ANALYSIS OF THE ACHIEVED RESULTS

The presented calculation results clearly show which value of the mean long-term service speed can be achieved by the ship or which value of probability of maintaining a given service speed on a given shipping route can be achieved at a service margin value assumed in design process of ship propulsion system (e.g. 15 %). Both the quantities for **K1** ship on different shipping routes are shown in Fig.18.

how large service margin for a given shipping route should be to maintain the set service speed at a given probability of its exceeding; it can be clearly observed when comparing the diagrams in Fig.18a and Fig.19. It means that in the case of applying the traditional method of determining the propulsion engine output power, with the use of service margin, percentage value of service margin for a given ship should be tightly correlated with statistical parameters of weather conditions on a given shipping route, and with an assumed probability of maintaining an assumed long-term service speed of ship.

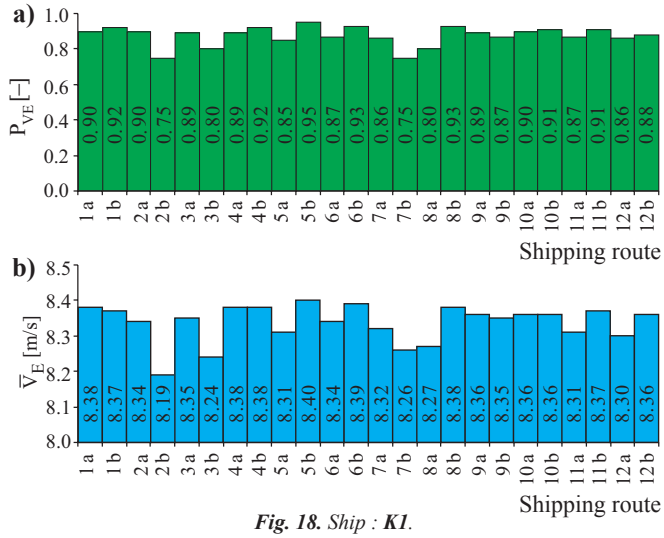

Fig. 18. *Ship : **K1**.*
a) *probability of maintaining the set service speed V_{ZE}*
b) *mean long-term service speed .*

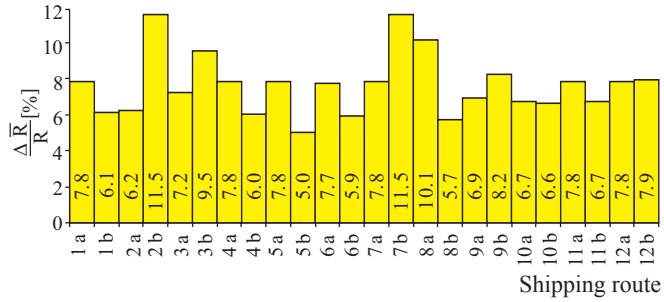

Fig. 19. *Index of additional resistance increase for **K1** ship, depending on shipping route .*

In Fig. 18 and 19 is presented an influence of shipping routes on the parameters associated with speed of **K1** ship. The same relations for the remaining ships can be found in [4].

In the next figures an influence of type and size of ship on the parameters associated with its speed on a given shipping route, is presented. As the considered ships differed to each other with regard to the contract speed V_K the following index of maintaining the set speed was introduced :

$$WP = \frac{\overline{V}_E}{V_{ZE}} \cdot 100\% \qquad (48)$$

The index makes it possible to more accurately compare performance of particular ships on a given shipping route. In Fig. 20 ÷ 25 are presented : the probability, P_{V_E} , of maintaining the set service speed V_{ZE} , the index WP acc. (48), as well as the index of increase of additional resistance acc. (46), for bulk carriers and containerships, respectively.

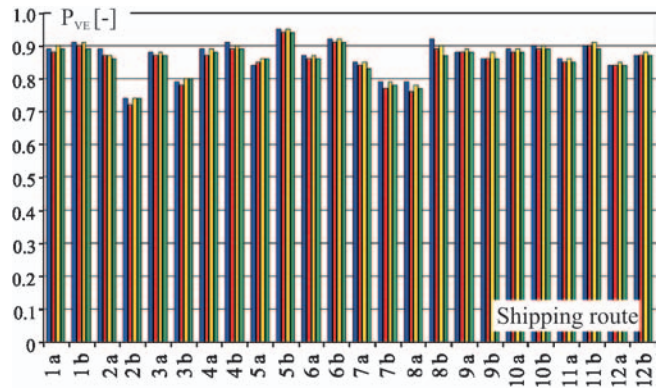

*Fig. 20. Probability of maintaining the set service speed V_{ZE} of bulk carriers : **blue** - M1; **red** - M2; **yellow** - M3; **green** - M4 .*

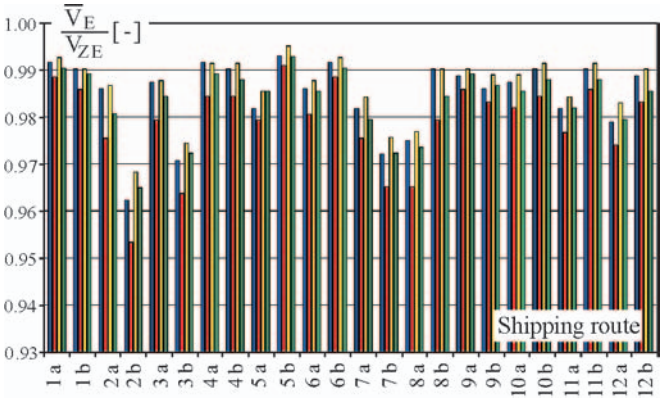

Fig. 21. *Index of maintaining the set service speed V_{ZE} of bulk carriers : **blue** - M1; **red** - M2; **yellow** - M3; **green** - M4 .*

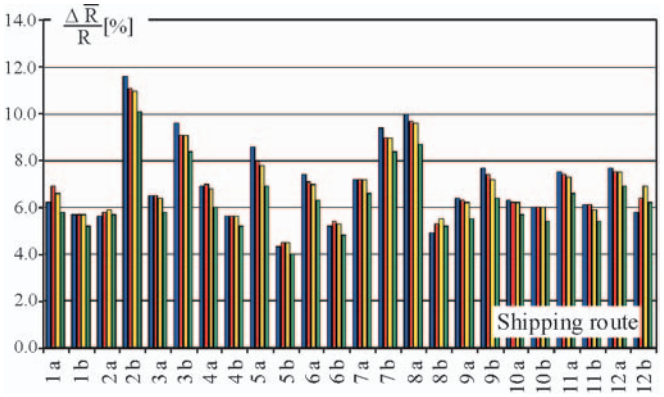

Fig. 22. *Index of additional resistance increase for bulk carriers : **blue** - M1; **red** - M2; **yellow** - M3; **green** - M4 .*

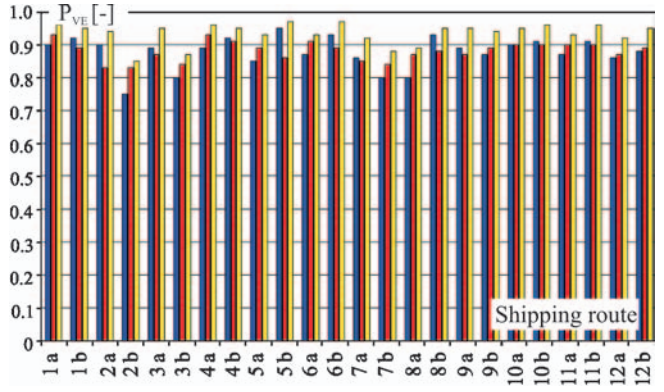

Fig. 23. *Probability of maintaining the set service speed V_{ZE} of containerships : **blue** - K1; **red** - K2; **yellow** - K3 .*

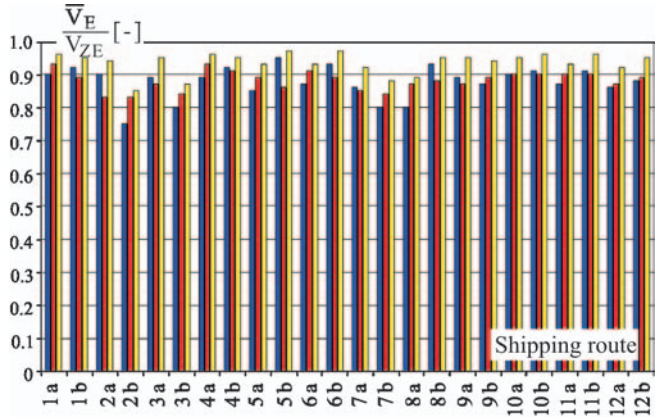

Fig. 24. *Index of maintaining the set service speed V_{ZE} of containerships : **blue** - K1; **red** - K2; **yellow** - K3 .*

From comparison of the diagrams it results that the performance of the ships on a considered shipping route differs to each other. Some ships show a greater value of the probability, P_{V_E},

of maintaining the set service speed V_{ZE}, and a greater value of the index WP than those showed by other ships. It speaks for different effectiveness of their propulsion systems.

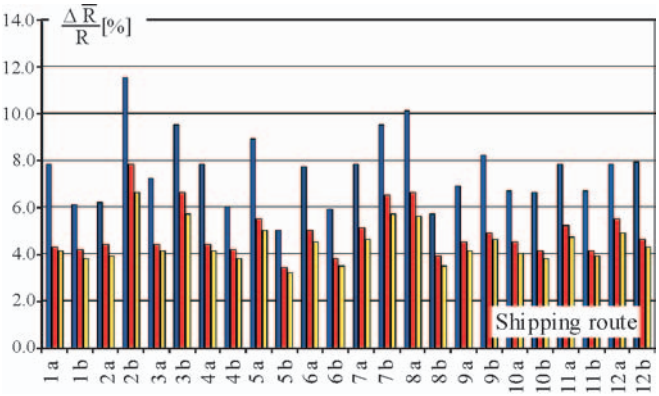

Fig. 25. Index of additional resistance increase for containerships : ***blue*** *- K1;* ***red*** *- K2;* ***yellow*** *- K3 .*

In the traditional designing of ship propulsion system and determining of service margin value (e.g. on the level of 15% [3,4]) the set service speed in real weather conditions is assumed lower than the contract speed by about 1 knot (for ships of the contract speed up to 20 knots). Hence for **K1** ship were performed calculations of the probability, P_{VE}, of maintaining a set service speed for its two values :

$$\Rightarrow V_{ZE} = V_K$$

$$\Rightarrow V_{ZE} = V_K - 1 \text{ [kn]}$$

and their results presented in Fig. 26.

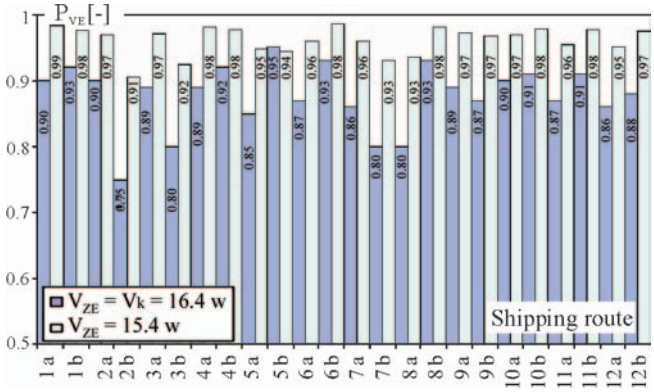

Fig. 26. Probability of maintaining the set service speed V_{ZE} of ***K1*** *ship .*

In the second case (i.e. $V_{ZE} = V_K - 1$ [kn]) the probability P_{V_E} for many shipping routes is close to 1, that is in compliance with the current designing practice and to a certain extent confirms (and verifies) accuracy of the performed calculations.

A PROPOSAL OF DEFINITION OF SERVICE MARGIN

On the basis of the performed calculations and conclusions resulting from the diagrams in Fig. 18 ÷ 25 was elaborated a proposal of definition of the service margin which associates a set service speed with probability of its maintaining on a given shipping route during a long time period.

Proposed definition of the service margin $k_ż$ (which determines surplus of engine output power)

For a given ship sailing on a given shipping route, the service margin $k_ż$ should have such percentage value as the ship in assumed loading conditions and assumed state of its hull and propeller surface, would be able to maintain the service speed, V_{ZE}, assumed in the frame of long-term prediction, at the assumed exceeding probability P_{VE}.

The definition concerns a designed ship intended for sailing on a given shipping route, however it can be also generalized to cover an arbitrary sailing region.

It should be observed that :

- too large value of V_{ZE} relative to V_K (contract speed) or too large value of the probability P_{VE} may cause that $k_ż$ would take large values and such ship would appear operationally unprofitable for its owner
- a reasonable (smaller) value of V_{ZE} may cause that at a reasonable value of $k_ż$, the probability P_{VE} would reach the value of one ($P_{VE} = 1$).

The above given comments mean that ship owner, when ordering a ship, should be aware of :

- a value of the long-term service speed he expects to be reached and
- at which level of its maintaining probability the designed ship would appear operationally profitable for him.

For the so defined service margin were performed calculations aimed at determination of its percentage value depending on shipping route under assumption that the set service speed V_{ZE}, maintained during long time period, will be equal to V_K ($V_{ZE} = V_K$) with the probability $P_{VE} = 0.95$.

The results of service margin calculations for **K1** ship in function of shipping route are presented in Fig.27.

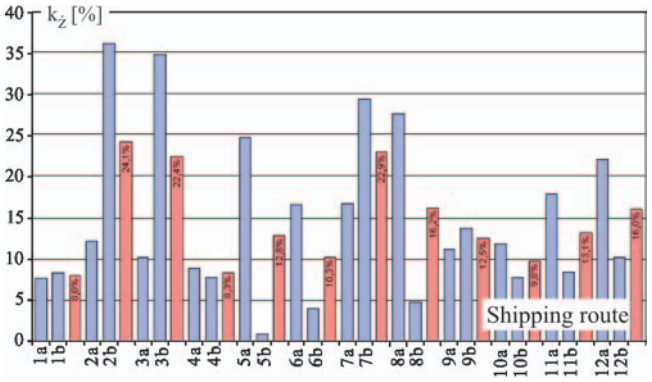

Fig. 27. The service margin $k_ż$ calculated for ***K1*** *ship in function of shipping route, for $V_{ZE} = V_K$ and $P_{VE} = 0.95$;* ***blue*** *- service margin for one-leg voyage of the ship;* ***red*** *- mean service margin for a shipping route .*

CONCLUSIONS

From the performed calculations the following conclusions can be drawn :

- Additional resistance of ship and its mean service speed depend on statistical weather parameters of shipping routes, hence ship service parameters depend on a kind of shipping route hence full utilization of statistical long-term parameters of waves and winds makes more accurate predicting ship service speed on a given route, possible.

- Influence of ship's type and size on its service parameters (resistance, speed) is observable but not so great as that of shipping route, but definite differences in effectiveness of the same ship on a given shipping route can be observed, that speaks for different quality (perfection) of designed propulsion systems.

- Service margin's value can be determined on the basis of ship service speed assumed by ship owner and probability of its maintaining on a given shipping route, hence it is not to have a constant value for a given shipping route, but it may result from targets and strategy which ship owner would apply to a given ship.

On the basis of the presented method was elaborated a computer software which may be also used for the following purposes :

- Comparison and assessment of ship designs as well as existing ships from the point of view of their service costs
- Optimization of a shipping route for a ship, especially in rough weather conditions
- Investigation of many other service parameters of ship and its equipment, e.g. frequency of using ship's steering gear on a given shipping route.

Calculation results obtained in the frame of long-term prediction of ship service parameters will be presented in separate papers.

NOMENCLATURE

$f(V_i)$ – probability distribution function of occurrence of the instantaneous ship speed V_i
$f(\Delta R_i)$ – probability distribution function of occurrence of the instantaneous additional resistance ΔR_i
f_A – probability of ship's staying in a given sea area A
f_ψ – probability of ship's sailing with the speed V and course angle ψ
k_z – service margin
n_R – number of intervals for additional resistance
n_V – number of intervals for ship speed
PR – relative increase of resistance
P_{TR} – total occurrence probability of the additional resistance ΔR of a given value
P_{TV} – total probability of developing the speed V by a ship at occurrence of the additional resistance ΔR
P_{VE} – probability of developing by a ship the set service speed V_E
R – still-water ship resistance
R^2 – share of the "resolved" variance
V_E – service speed
$\overline{V}_E$ – average long-term service speed of a ship sailing on a given shipping route
V_k – contract speed
V_{ZE} – set service speed
WP – index of maintaining the set service speed
ΔR – additional resistance resulting from rough weather conditions
$\Delta\overline{R}$ – statistical average value of additional resistance
ψ – geographical angle of ship course.

BIBLIOGRAPHY

1. *Atlas Weltmeer* : VEB Herman Haack, Geographisch--Kartographische Anstalt Gotha, 1989
2. Jóźwiak J., Podgórski J. : *Essentials of statistics* (in Polish). Polish Economic Publishers (Polskie Wydawnictwo Ekonomiczne). Warszawa, 2001
3. Szelangiewicz T., Żelazny K. : *Calculation of ship resistance and speed in the frame of long-term prediction* (in Polish). International Scientific Technical Conference EXPLO-SHIP 2006. Szczecin-Kopenhaga, May 2006
4. Żelazny K. : *Numerical prediction of mean long-term service speed of transport ship* (in Polish) Doctorate thesis, Maritime Technology Faculty, Szczecin University of Technology, 2005

CONTACT WITH THE AUTHORS
Prof. Tadeusz Szelangiewicz
Katarzyna Żelazny, D.Sc., Eng.
Faculty of Marine Technology,
Szczecin University of Technology
Al. Piastów 41
71-065 Szczecin, POLAND
e-mail : tadeusz.szelangiewicz@ps.pl

Miscellanea

The Foundation for Safety and Environment Protection

25 years of training on manned ship models

In 1981 in Iława (Silm lake) on the basis of agreement between the then Maritime High School, Gdynia, and Gdańsk University of Technology was commenced regular education activity aiming at training ship masters, first officers and pilots in ship manoeuvring. The trainings were based on large manned floating ship models equipped with devices simulating operation of the ship systems engaged in manoeuvring. The first training model representing a tanker is one out of nine models used today for training courses. As the years go construction and outfitting of models as well as training water areas, at first simple and sparse, have been becoming more and more perfect and better adjusted to fulfilling their role. Also, organizational form of the training has been changed - in 1989 the Foundation for Safety and Environment Protection, Iława, was established by both the universities with the aim of carrying out trainings and research in the area of safety at sea.

In spite of many difficulties due to objective external factors and sometimes a pessimism as to purposefulness of developing the methods based on models (in the times of proliferation of computer simulation) the Centre in Iława today ranks as one of the best worldwide, equipped with the most suitable training models and water areas providing the widest training possibilities. Also, an unique approach to realization training tasks has been elaborated. As a result the use of vacancies in training courses reaches 100%, and representatives of many countries and organizations are turning to the Centre for advise or directly for realization of a similar undertaking on their territory. So far, as many as 2600 ship masters, first officers and pilots from almost 40 countries and all continents have taken part in various training courses in Iława.